Geological Society of America Bulletin

Mechanics of V-shaped conjugate strike-slip faults and the corresponding continuum mode of continental deformation

An Yin and Michael H. Taylor

Geological Society of America Bulletin published online 3 March 2011;
doi: 10.1130/B30159.1

Geological Society of America Bulletin, published online on 3 March 2011 as doi:10.1130/B30159.1

Mechanics of V-shaped conjugate strike-slip faults and the corresponding continuum mode of continental deformation

An Yin[1,2,†] and Michael H. Taylor[3]

[1]*Department of Earth and Space Sciences and Institute of Geophysics and Planetary Physics, University of California, Los Angeles, California 90095-1567, USA*

[2]*Structural Geology Group, China University of Geosciences (Beijing), Beijing 100085, China*

[3]*Department of Geology, University of Kansas, Lawrence, Kansas 66045, USA*

ABSTRACT

V-shaped conjugate strike-slip faults occur widely on Earth, Venus, and Mars in the solar system. They commonly lie at 60°–75° in map view from the maximum compressive stress (σ_1) direction. This fault pattern cannot be explained directly by the Coulomb fracture criterion, which predicts the formation of X-shaped shear fractures at 30° from the σ_1 direction. Possible explanations of this odd fault geometry include rotation of early formed Coulomb fractures or reactivation of preexisting weakness. Here, we show that none of these mechanisms is feasible for the formation of a late Cenozoic conjugate strike-slip fault system in central Tibet. Instead, its initiation can be best explained by distributed deformation during the formation of two parallel and adjoining shear zones that have opposing senses of shear. Our suggestion is based on the current global positioning system (GPS) velocity field in Tibet, which can be divided into two east-trending shear zones: a northern left-slip zone consisting of active ENE-striking left-slip faults, and a southern right-slip zone consisting of active WNW-striking right-slip faults. The correlation between the GPS strain field and the fault pattern suggests that the central Tibet conjugate faults may have initiated as two sets of Riedel shears in the two parallel but separate shear zones. Because the two east-trending shear zones also experience north-south contraction, we refer to this mechanism of conjugate-fault formation as paired general-shear (PGS) deformation. Assuming a Newtonian fluid, the observed Tibetan GPS velocity field requires the paired shear zones to have formed either by gravitational spreading of the Tibetan lithosphere or a horizontal shear at the base of the upper crust or mantle lithosphere. We demonstrate the feasibility of the two inferred mechanisms for the formation of V-shaped conjugate faults using simple sandbox experiments. Our paired general-shear (PGS) model implies that the combined effect of the state of strain and the state of stress favors only one set (i.e., Riedel shear) of Coulomb conjugate shear fractures under general shear flow. It also requires continuum deformation rather than discrete extrusion tectonics as the most dominant mode of deformation during the late Cenozoic development of the central Tibetan Plateau.

INTRODUCTION

The Coulomb fracture criterion predicts the formation of X-shaped conjugate faults oriented at ~30° from the maximum compressive stress (σ_1) direction (Fig. 1A). Early workers such as Anderson (1942), Freund (1970), and Sylvester (1988) all noted that such a fault pattern is not stable during finite-strain deformation. At a scale of hundreds to thousands of kilometers, conjugate strike-slip faults hosted by continental lithosphere rarely exhibit X-shaped geometry; rather, they commonly display V-shaped configurations in map view (Fig. 1A) (Taylor and Yin, 2009; Yin, 2010). V-shaped conjugate strike-slip faults are particularly well developed in collisional orogens on Earth, including those in the eastern Alps (Ratschbacher et al., 1991a, 1991b), western Turkey (Sengor and Kidd, 1979; Jackson and McKenzie, 1984; Dhont et al., 2006), northern Afghanistan (Tapponnier et al., 1981; Brookfield and Hashmat, 2001), central Tibet (Yin et al., 1999; Yin, 2000; Taylor et al., 2003; Taylor and Yin, 2009), northern Iran (Alavi, 1994; Allen et al., 2004; Copley and Jackson, 2006; Guest et al., 2006), central Mongolia (e.g., Calais et al., 2003; Cunningham, 2005; Walker et al., 2007; Yin, 2010), Indochina (Leloup et al., 1995), and the Gulf of Thailand (Morley, 2001; Morley et al., 2001; Kornsawan and Morley, 2002) (Fig. 1B). Besides collisional orogens, V-shaped conjugate strike-slip faults are also documented in arc systems such as in the Venezuela Andes (e.g., Backé et al., 2006; Escalona and Mann, 2006). On Venus, several sets of V-shaped conjugate strike-slip shear zones occur around the edges of Lakshmi Planum in the Ishtar Terra (e.g., Ivanov and Head, 2008). On Mars, a possible pair of V-shaped conjugate faults occurs in the southeastern Tharsis rise, comprising the right-slip Clarita Fossae fault zone and the left-slip Valles Marineris fault zone (Montgomery et al., 2009).

V-shaped conjugate strike-slip faults as exemplified by the central Tibet conjugate fault zone (Taylor et al., 2003) have the following characteristics: (1) They lie at 60°–75° from the maximum compressive stress (σ_1) direction; (2) All V's defined by fault mergers are aligned parallel to each other and open in the downslope direction of regional topography (i.e., the thinning direction of the crust, assuming it is in Airy isostasy); (3) Conjugate faults terminate at their merging points (i.e., the tips of the V's) where strike-slip motion vanishes; (4) Two sets of conjugate faults were initiated at about the same time.

For an ideal situation, the two sets of conjugate faults should also have comparable slip over their entire history. In reality, the total slip magnitude of each fault set may vary considerably due to differential slip histories on individual faults. For example, after initiation of a V-shaped conjugate strike-slip fault system, the two fault sets could have experienced regional rotation

†E-mail: yin@ess.ucla.edu; ayin54@gmail.com.

 doi: 10.1130/B30159.1; 15 figures.

Geological Society of America Bulletin, published online on 3 March 2011 as doi:10.1130/B30159.1

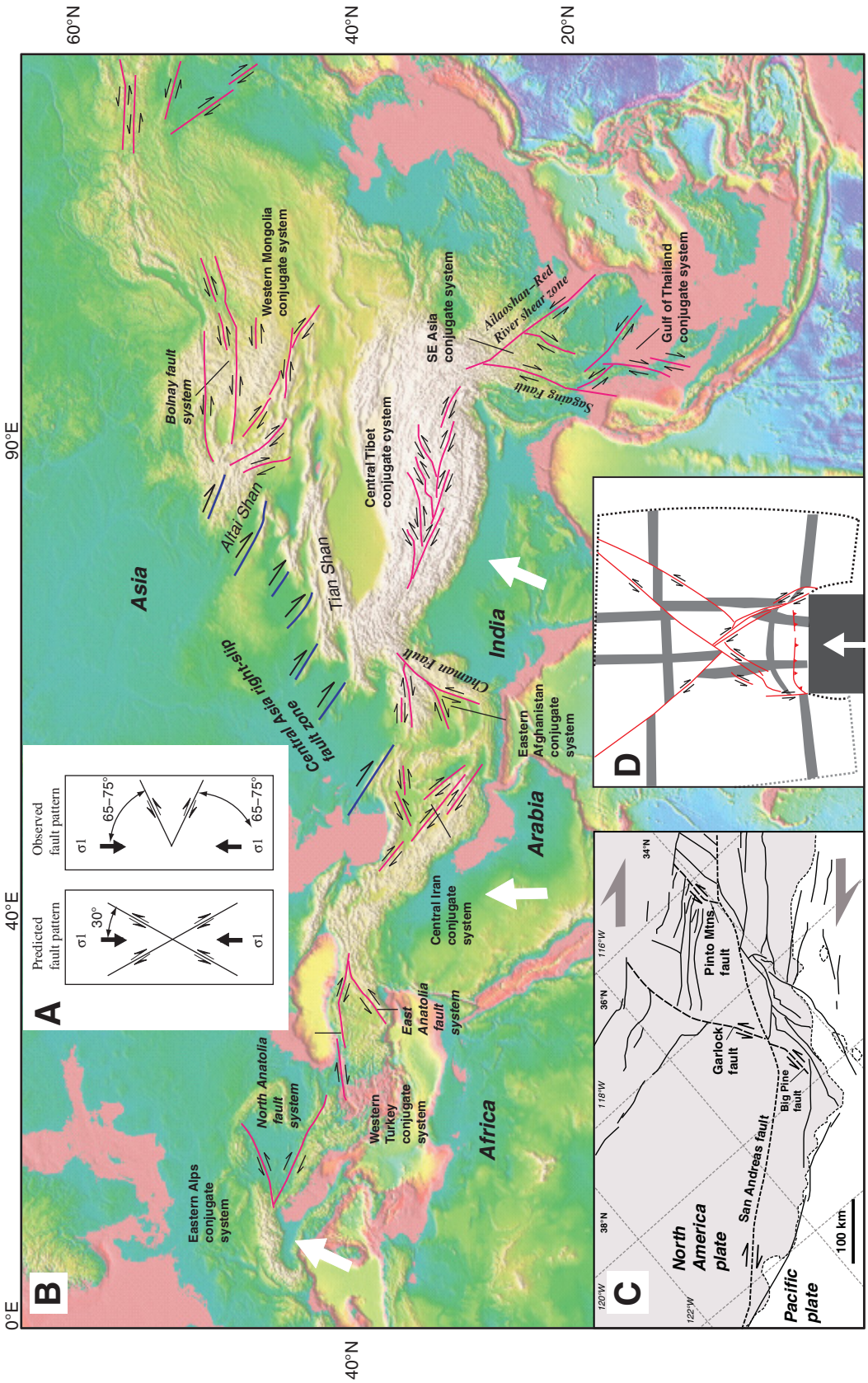

Figure 1. (A) Conjugate fault orientations predicted by the Coulomb fracture criterion (left) versus observed fault orientations and the maximum principal stress direction (σ_1) across the Alpine-Himalaya-Tibet collision zone (right). (B) Distribution of major V-shaped conjugate strike-slip faults in the Alpine-Himalaya-Tibet collision zone, slightly modified from Yin (2010). (C) Major strike-slip faults in the simple-shear–dominated San Andreas transform system in southern California, redrawn from Powell (1993). (D) Results of an analogue experiment showing X-shaped conjugate strike-slip faults generated by indentation of a rigid block into a thin layer of sand, redrawn from Peltzer (1988).

Geological Society of America Bulletin, published online on 3 March 2011 as doi:10.1130/B30159.1

that was accommodated by further slip of different amounts on each fault (Mandl and Fernandez Luque, 1970; Mandl, 1987, 1988). Alternatively, one set of the conjugate faults may be weaker and thus moves more rapidly, resulting in a greater total slip when compared to the other set of the conjugate faults with a higher mechanical strength. The discussion in this paper focuses mainly on how V-shaped conjugate faults were initiated mechanically rather than how they may have developed kinematically.

Although the classic San Andreas system and nearby antithetic left-slip faults such as the Garlock fault form apparent V-shaped fault geometry, we do not consider them as V-shaped conjugate fault systems because they were initiated at very different times and their initiation may have been driven by different mechanisms. That is, the San Andreas system started before 20 Ma related to relative plate motion, while the Garlock fault began to be active after ca. 10 Ma related to differential Basin-Range extension (Fig. 1C) (e.g., Davis and Burchfiel, 1973; Powell, 1993; McGill and Sieh, 1991, 1993; Guest et al., 2003).

Despite their wide occurrence on terrestrial planets, the mechanical origin of V-shaped conjugate strike-slip faults has never been investigated. Existing work concerns mainly their kinematic roles in accommodating lateral extrusion of continental lithosphere (e.g., Tapponnier et al., 1986; Ratschbacher et al., 1991a; Leloup et al., 1995). These extrusion models have been successful in explaining regional tectonic histories, but they are unable to reproduce the observed fault orientations using analogue models (Fig. 1D) (Tapponnier et al., 1982; Davy and Cobbold, 1988; Peltzer and Tapponnier, 1988; Peltzer, 1988; Ratschbacher et al., 1991b; Fournier et al., 2004). In this paper, we address the reasons that conjugate strike-slip faults form at exceptionally high angles to the maximum compressive stress direction by presenting a new mechanism that we term the paired general-shear (PGS) model. The main thesis of our new model is that V-shaped conjugate strike-slip faults were initiated by the development of two sets of Riedel shears during the evolution of two parallel and adjoining shear zones that have opposite senses of shear. Our model implies that the combined effect of the state of strain and the state of stress dictates the selection of Coulomb conjugate fractures (i.e., one set becomes active while the other set remains inactive during finite-strain deformation). Our mechanical analysis also indicates that the central Tibetan Plateau, hosting discrete V-shaped conjugate fault systems (a few kilometers wide and hundreds of kilometers long for individual faults), must have deformed in a continuum fashion in the late Cenozoic, a conclusion consistent with the thin-viscous sheet model of England and Houseman (1986).

Here, we first review the existing models (Fig. 2) that may explain the formation and development of the central Tibet conjugate fault zone (Figs. 3, 4, and 5). This is followed by an analysis of the Tibetan GPS velocity field and its relationship to the active central Tibet conjugate fault zone. Using spatial correlation between the Tibetan GPS velocity field and fault patterns, we show that paired general-shear deformation can lead to the development of V-shaped conjugate faults. Finally, we discuss the general implications of our model for the formation of low-angle normal faults and high-angle reverse faults.

PREVIOUS HYPOTHESES

Vertical-Axis Rotation (VAR) Models

V-shaped conjugate strike-slip faults could have been initiated at ~30° from the σ_1 direction and then rotated about vertical axes to their current orientations (Figs. 2A–2D) (Freund, 1970; Ron et al., 1984; McKenzie and Jackson, 1986; Dewey et al., 1989). Fault rotation might have been accommodated by (1) bookshelf faulting (Fig. 2A) (Mandl, 1987; Cobbold and Davy, 1988; England and Molnar, 1990), (2) pure-shear deformation (Fig. 2B) (Dewey et al., 1989), (3) unidirectional extension (Fig. 2C), and/or (4) unidirectional contraction (Fig. 2D). In the bookshelf-faulting model, the magnitude of fault slip (*d*) is proportional to the magnitude of vertical-axis rotation (φ) and fault spacing (*W*) (Fig. 2A). In central Tibet, the average fault spacing is 120–150 km (Taylor et al., 2003). Thus, a 40° rotation of Coulomb faults to their current orientations would require a fault slip of >90 km. This predicted fault slip far exceeds the observed 12–20 km of fault slip from central Tibet (Taylor et al., 2003) (Fig. 5). Fault rotation by pure-shear deformation (Fig. 2B) would require −65% and 65% contractional and extensional strain, after the initiation of the conjugate faults. Finally, fault rotations by unidirectional extension (Fig. 2C) or contraction (Fig. 2D) require 375% of extension or −79% of contraction.

To place the distributed deformation models in the context of Tibetan geology, we consider three end-member situations: (1) closely spaced east-trending thrusts and folds coeval with conjugate faulting (Fig. 6A), (2) closely spaced northwest-trending right-slip faults and northeast-trending left-slip faults (Fig. 6B), and (3) closely spaced north-trending normal faults (Fig. 6C). For the first possibility, thrusts and folds coeval with V-shaped conjugate faults should be present within fault-bounded wedges that open to the east in central Tibet (Fig. 3). However, geologic mapping in the past decade from central Tibet indicates that early Tertiary east-trending thrusts and folds are cut by active left-slip faults in the Qiangtang terrane (Yin et al., 1999; Taylor et al., 2003; Kapp et al., 2000, 2003a, 2005a) and by active right-slip faults in the Lhasa terrane (Taylor et al., 2003). The second possibility is also unlikely because distributed strike-slip deformation is lacking across central Tibet (Taylor et al., 2003; Kapp et al., 2005a). Although there are minor north-trending normal faults present in the fault-bounded wedges in central Tibet (Fig. 4A), their magnitude of slip must be less than 5 km, assuming the normal faults dip at 60°. This is because Jurassic strata with a maximum thickness of ~4 km (Xizang BGMR, 1993) are present on both sides of the rift-bounding faults (Fig. 5A). Sparse presence of minor normal faults and the small (<5 km) magnitude of slip are incapable of accommodating the large amount of strain required for fault rotation models.

Although significant vertical-axis rotation is unlikely in central Tibet based on these structural tests, we do not rule out large rotation occurring elsewhere in the Indo-Asian collision zone, as anticipated in the model of Cobbold and Davy (1988). In fact, paleomagnetic studies and palinspastic reconstructions indicate up to 40° of vertical-axis rotation across Central Asia (Cobbold et al., 1989; Thomas et al., 1993, 1994, 1996; Bourgeois et al., 1997).

Preexisting Weakness

Preexisting weakness may impose anisotropy and thus produce non-Coulomb fault geometry (e.g., Donath, 1961; Sibson et al., 1988; Yin and Ranalli, 1992). This mechanism cannot apply to the Lhasa terrane in southern Tibet (Fig. 3), because it was dominated by pre-Cenozoic east-trending structures, sedimentary facies, and plutonic belts (e.g., Yin et al., 1994; Murphy et al., 1997; Yin and Harrison, 2000; Kapp et al., 2003b). All of these features are cut obliquely by the late Cenozoic strike-slip faults (Fig. 5A) (Taylor et al., 2003).

The Qiangtang terrane in northern Tibet (Fig. 3) is dominated by ENE-striking active left-slip faults that cut the older east-plunging Qiangtang anticlinorium, the most dominant structure in that area (Kapp et al., 2000, 2003a, 2005a). Early east-striking Paleogene thrusts are also cut by the active ENE-striking left-slip faults (Fig. 5B) (Taylor et al., 2003).

Sequential Deformation

Although an orthogonal switch in the σ_1 direction could have occurred and caused reactivation and slip reversal of early formed Coulomb-type faults (Fig. 2E), we are not aware

Geological Society of America Bulletin, published online on 3 March 2011 as doi:10.1130/B30159.1

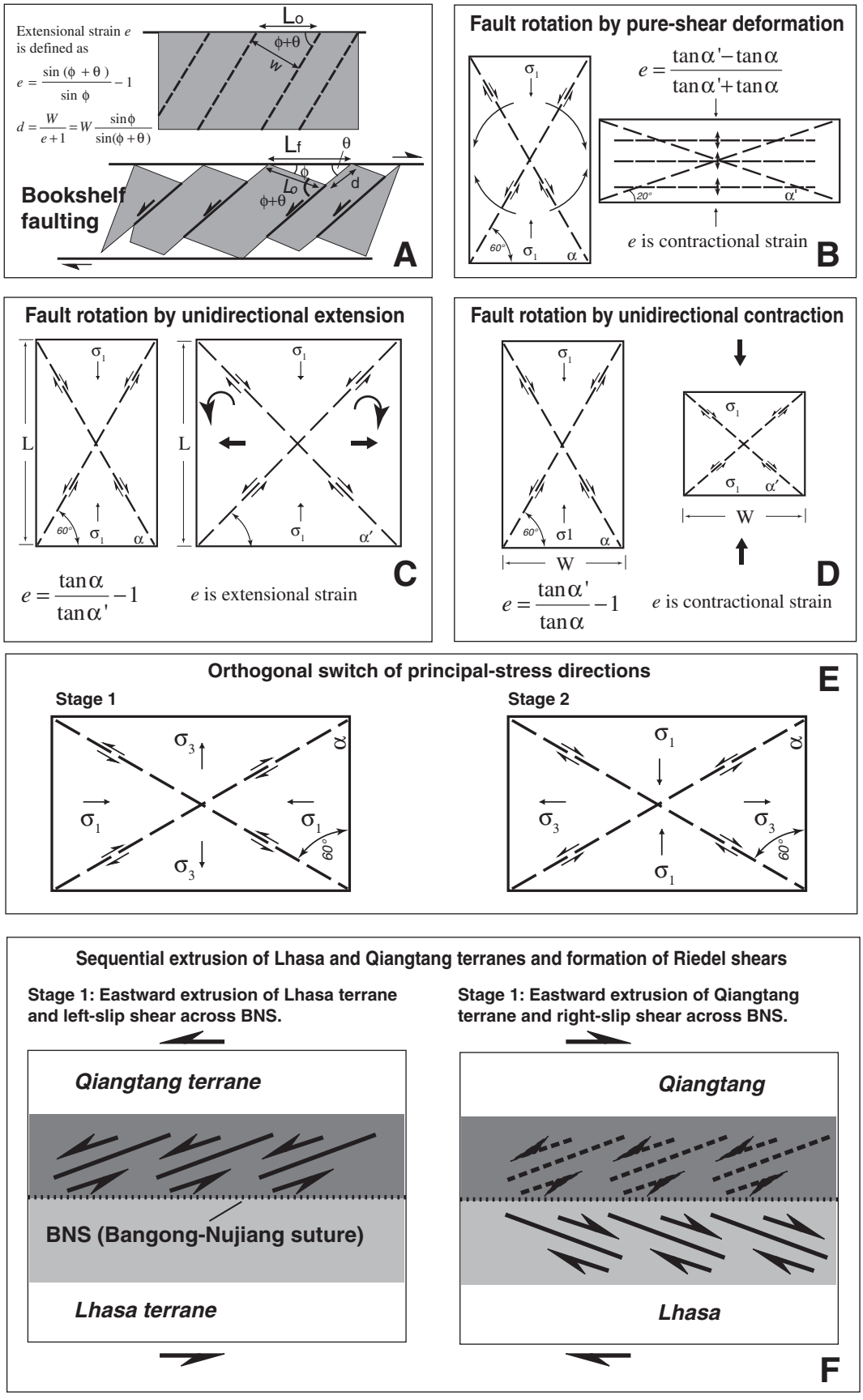

Figure 2 (*Continued on following page*).

Geological Society of America Bulletin, published online on 3 March 2011 as doi:10.1130/B30159.1

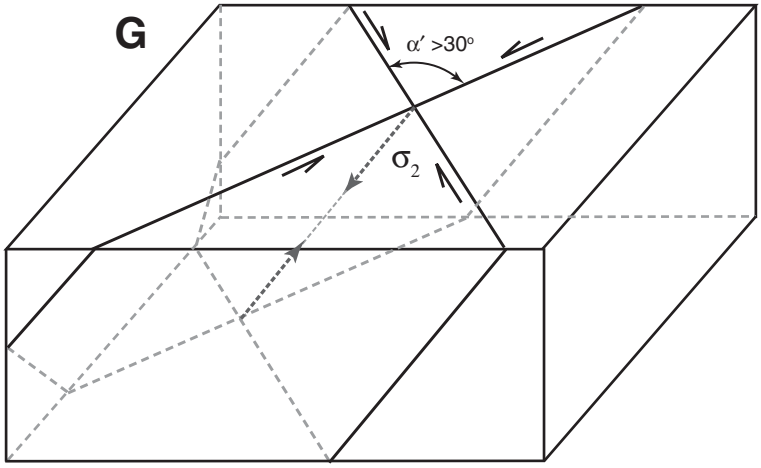

Figure 2 (*Continued*). Kinematic models illustrating the formation of non-Coulomb–type conjugate strike-slip faults. (A) Fault rotation via bookshelf-style faulting. (B) Fault rotation via distributed pure-shear deformation by combined contractional and extensional deformation. (C) Fault rotation by distributed unidirectional extension. (D) Fault rotation by distributed unidirectional contraction. (E) Formation of non-Coulomb–type faults by an orthogonal switch of principal stresses. (F) Sequential extrusion model predicting eastward extrusion of the Lhasa terrane first, followed by eastward extrusion of the Qiangtang terrane to the north. (G) Three-dimensional effect of Coulomb conjugate faults intersecting the ground surface.

of any geologic observations that support such a Cenozoic tectonic history in Tibet.

The lateral extrusion model predicts sequential northward activation of eastward-extruding blocks across Tibet (Tapponnier et al., 1982; Peltzer and Tapponnier, 1988). In this model, first eastward extrusion of the Lhasa block could have produced left-slip shear and ENE-trending left-slip Riedel fractures in the Qiangtang terrane (Fig. 2F). The subsequent extrusion of the Qiangtang terrane could have produced right-slip shear and WNW-trending right-slip Riedel fractures (Fig. 2F). This model requires left-slip faults in the Qiangtang terrane to be currently inactive (Armijo et al., 1986, 1989), which is inconsistent with geophysical and geologic observations (Molnar and Lyon-Caen, 1989; Taylor et al., 2003).

In simulating collisional tectonics, several workers show that early Coulomb-type strike-slip faults in front of an indenter could evolve into oblique strike-slip faults with obtuse intersection angles facing the maximum compressive stress directions (Cobbold and Davy, 1988; Richard and Cobbold, 1990; Jolivet et al., 1990; Ratschbacher et al., 1991b; Casas et al., 2001). For the conjugate strike-slip faults we studied in central Tibet, we found no evidence for such a transition in fault kinematics. In fact, motion on most of the late Cenozoic strike-slip faults has a small component of fault-perpendicular extension (Taylor et al., 2003).

Initiation of Conjugate Strike-Slip Faults at Obtuse Angles

When the three principal stresses are neither horizontal nor vertical, the induced conjugate strike-slip fault planes are not vertical, and thus their intersections with Earth's surface may exhibit an apparent obtuse angle in the compressive quadrants (Fig. 2G). This possibility was raised by Kapp and Guynn (2004). However, our field observations suggest that active strike-slip faults all have nearly vertical orientations, as indicated by their straight traces in map view and high-angle geometry in cross sections (Figs. 4A and 5). Offset of morphologic features (Taylor et al., 2003) and direct observations of fault striations (Fig. 4B) also suggest that motion on V-shaped conjugate faults in central Tibet is nearly pure strike slip.

PAIRED GENERAL SHEAR (PGS) MODEL

Fault formation depends not only on the state of stress, but also on the commonly neglected state of strain. For example, classically disposed conjugate faults may be initiated under the Coulomb fracture mechanism when the strain state is coaxial (Fig. 7A). In contrast, more complicated shear fracture patterns, though also controlled by the Coulomb fracture mechanism, may be initiated when the strain state is noncoaxial (i.e., P, R, and R′ shears) (Tchalenko, 1970; Wilcox et al., 1973) (Fig. 7B). Naylor et al. (1986) expanded the simple-shear experiments of Tchalenko (1970) and Wilcox et al. (1973) and showed that Riedel shears (R) can also form under the condition of general shear that combines simple-shear and pure-shear strains (e.g., Simpson and DePoar, 1993). To evaluate whether coaxial or noncoaxial progressive deformation is responsible for the development of a particular type of fault system, we need to establish displacement or velocity fields at the time of fault formation. This may be accomplished for an active fault system that was initiated recently and has undergone steady-state deformation. This rationale led us to examine the relationship between the current GPS velocity field and the fault orientations of late Cenozoic conjugate strike-slip faults in central Tibet. This information, as illustrated next, provides a key insight into the formation mechanism of V-shaped conjugate strike-slip faults.

Tibetan GPS Velocity Field and its Physical Interpretation

Wang et al. (2001), Zhang et al. (2004), and Gan et al. (2007) documented uniform north-south shortening across Tibet based on GPS surveys (Fig. 8). The uniform shortening strain is expressed by a linear decrease in the magnitude of northward velocity relative to the fixed Eurasia (Fig. 8). Zhang et al. (2004) and Gan et al. (2007) noted that the Qiangtang terrane is undergoing east-trending left-slip shear, whereas the Lhasa terrane is undergoing east-trending right-slip shear (Fig. 8C). The boundary between the east-trending right-slip and left-slip shear zones lies along the central axis of the Tibetan conjugate strike-slip fault zone and coincides approximately with the Bangong-Nujiang suture zone (Figs. 3 and 8A). The GPS data also show that the maximum eastward velocity along the axis of the conjugate fault zone increases from about –4 mm/yr in the west to ~17 mm/yr in the east relative to fixed Eurasia as a result of east-west extension (Fig. 8C).

In order to understand how the current strain rate is distributed across Tibet, Allmendinger et al. (2007) calculated the average strain-rate tensor across a series of discrete domains using a spatial filter constant of 150 km. Their relatively coarse grid smeared some important kinematic features of active Tibetan deformation. For example, the division of the east-trending right-slip and left-slip shear zones recognized by Zhang et al. (2004) was completely filtered out in their strain calculations. Using much finer grids and denser GPS networks, Gan et al. (2007) also determined

Geological Society of America Bulletin, published online on 3 March 2011 as doi:10.1130/B30159.1

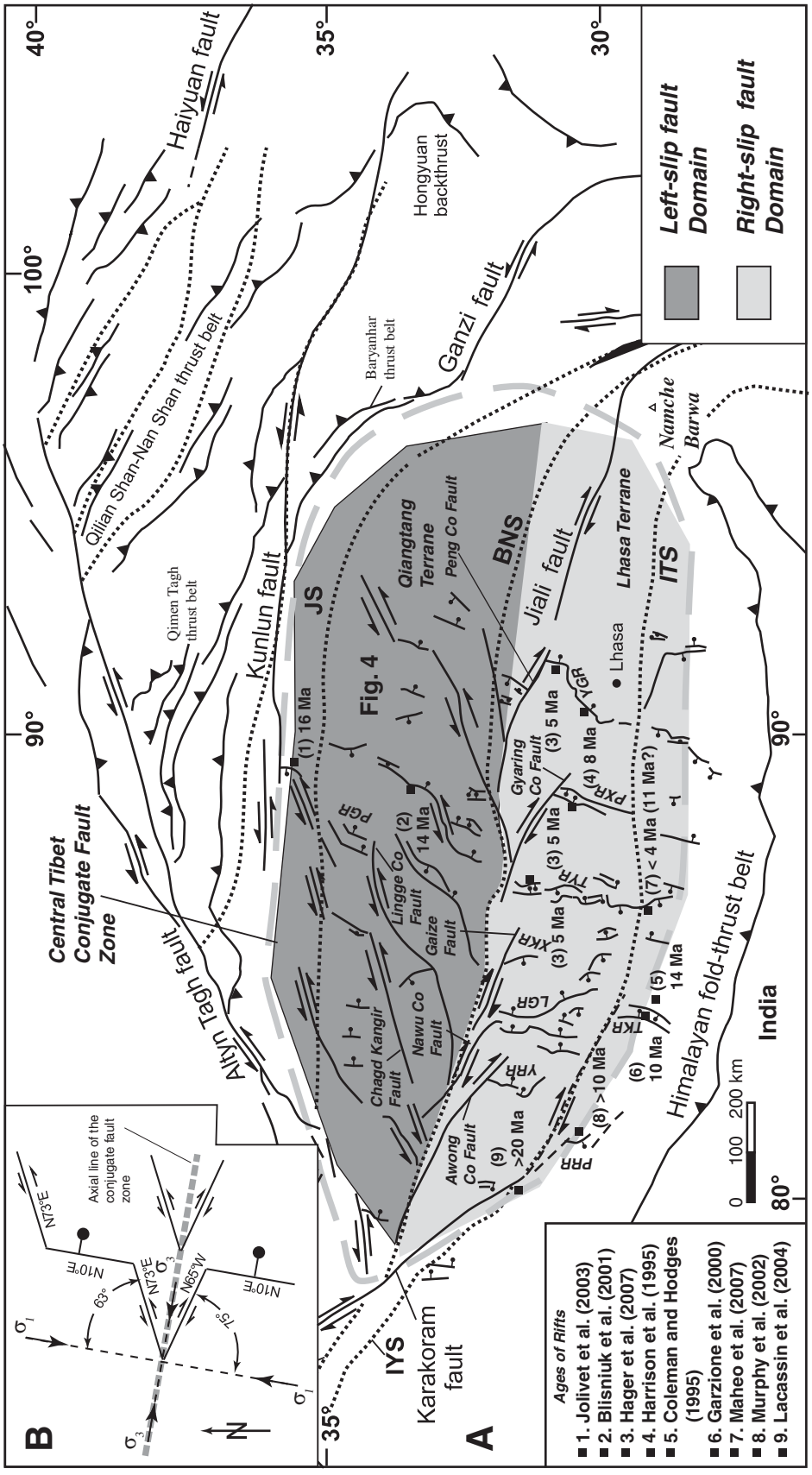

Figure 3. (A) Map of late Cenozoic conjugate strike-slip faults in central Tibet and age distribution of rift initiation across the region. Rift ages are from the following sources: (1) Jolivet et al. (2003), (2) Blisniuk et al. (2001), (3) Hager et al. (2007), (4) Harrison et al. (1995) and Kapp et al. (2005b), (6) Coleman and Hodges (1995), (7) Garzione et al. (2000) and Maheo et al. (2007), (8) Murphy et al. (2002), and (9) Lacassin et al. (2004). In general, rift initiation ages are oldest in the north, south, and west and become younger toward the interior and eastern part of central Tibet. Abbreviations for major rift systems are as follows: YGR—Yadong-Gulu rift; PXR—Pumqu-Xianza rift; TYR—Tangra Yum Co rift; XKR—Xiakangjian rift; LGR—Lunggar rift; YRR—Yari rift; PKR—Purong Kangri rift; ZSR—Zangser Kangir rift; PRR—Purang rift; TKR—Thakkola rift. Suture zones: JS—Jinsha suture; BNS—Bangong-Nujiang suture; ITS—Indus-Tsangpo suture. (B) (Inset map) Relationship between the orientations of conjugate faults in central Tibet and the direction of the maximum compressive stress inferred from the trends of major rifts.

Geological Society of America Bulletin, published online on 3 March 2011 as doi:10.1130/B30159.1

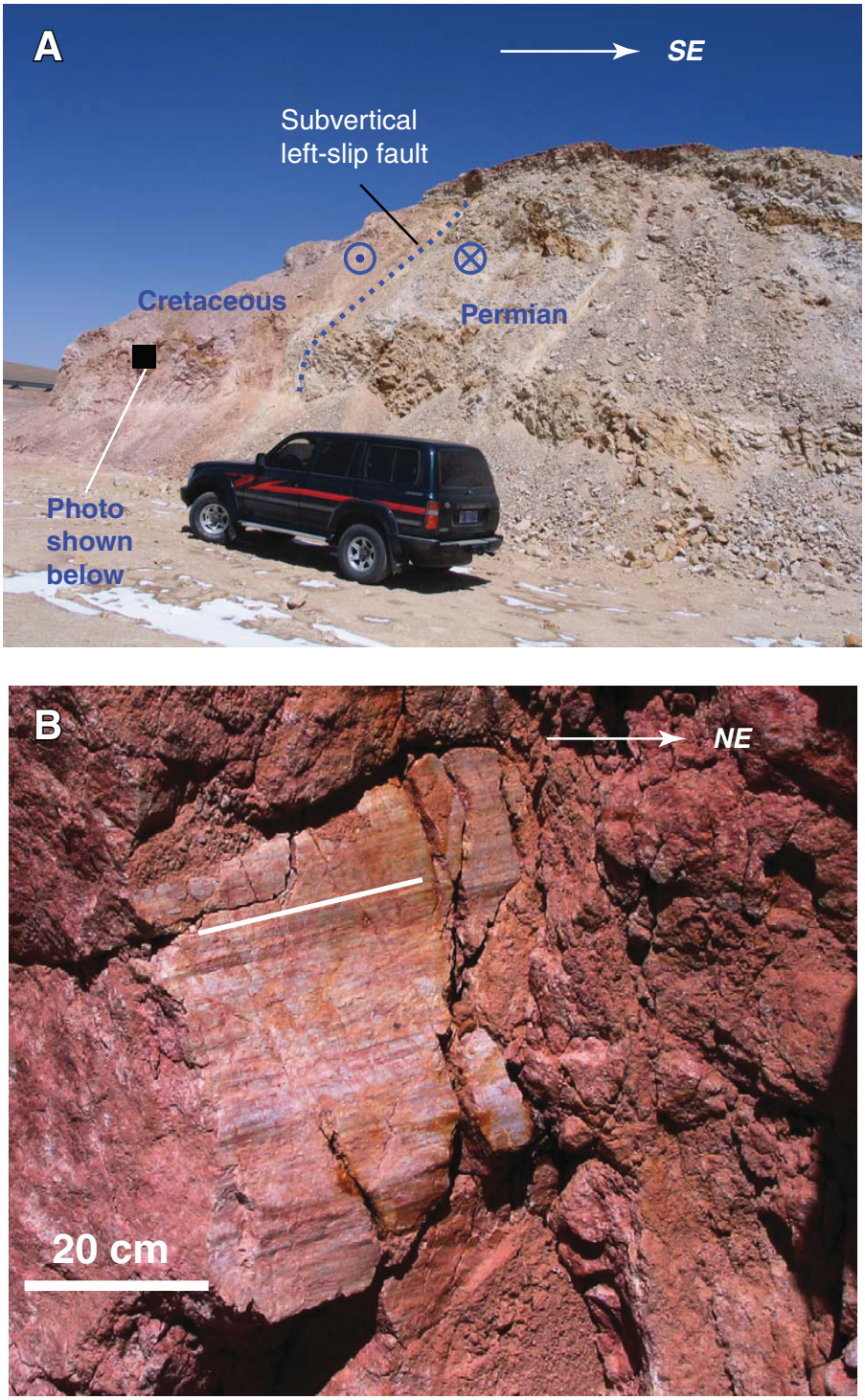

Figure 4. (A) Subvertical left-slip fault in the Qiangtang terrane juxtaposing Cretaceous red beds against Permian sandstone. See Figure 3 for location. (B) Subhorizontal striations on shear fractures in the same fault zone in Cretaceous strata.

the strain-rate and rotation-rate distributions across Tibet. They revealed the presence of two parallel east-trending shear zones with opposing senses of shear in central Tibet. Gan et al. (2007) attributed this finding to glacial-like flow driven by gravitational spreading of the Tibetan lithosphere. A similar conclusion was also reached by Copley and McKenzie (2007) in their dynamic modeling of Tibetan deformation.

The presence of two parallel shear zones with opposing senses of shear provides a key clue to the formation mechanism of the V-shaped conjugate faults in central Tibet. If shear deformation as depicted from the Tibetan GPS velocity field has persisted since the time when the conjugate fault zone was initiated in the late Cenozoic (i.e., 15–5 Ma; see summary in Fig. 3), then the odd fault geometry may be explained by the development of two sets of Riedel shears in two parallel and adjoining shear zones that have opposite senses of shear (Fig. 7D). Specifically, the formation of the east-trending left-slip shear zone in the Qiangtang terrane could have produced ENE-striking, left-slip faults, while the formation of the east-trending right-slip shear zone in the Lhasa terrane could have produced WNW-striking, right-slip faults (Fig. 3; cf. Fig. 7D). Because central Tibet is currently experiencing north-south contraction, the right-slip and left-slip shear zones in the Lhasa and Qiangtang terranes are general-shear zones rather than simple-shear zones (e.g., Simpson and DePoar, 1993).

An obvious question with this interpretation is why conjugate Riedel (R′) and primary shears (P) did not develop across central Tibet. It has long been known that R′ and P shears are present only in experiments using wet clay (e.g., Tchalenko, 1970; Wilcox et al., 1973) and are generally absent in dry sand under simple-shear or general-shear conditions (e.g., Naylor et al., 1986; Adam et al., 2005). Eisenstadt and Sims (2005) attributed this difference to the excessively high cohesive strength of wet clays. We think that this interpretation may be appropriate for the lack of P shears in simple-shear sandbox experiments, but an additional explanation is needed for the less favorable development of R′ shears under simple-shear deformation of dry sand. First, we assume that the initial R and R′ shear zones have finite widths. To initiate a discrete shear zone during finite-strain deformation, particles in the shear zone must experience rotation due to the concentration of shear stress along the potential shear fractures (i.e., a local velocity boundary condition). However, in the same region where the shear zones are to be created, there is also a rotational field imposed by the overall noncoaxial flow field (i.e., regional boundary condition) (Figs. 7E and 7F). Thus, whether a shear zone

Geological Society of America Bulletin, published online on 3 March 2011 as doi:10.1130/B30159.1

develops or not depends on the competition of the two rotational processes. For pure-shear deformation, this competition does not exist because vorticity is zero everywhere. Thus, the local boundary condition across the potential shear zones decides the direction and rate of rotation.

The situation for simple-shear deformation is quite different. Although the sense of shear across Riedel shear zones is the same as the rotational direction imposed by the regional simple-shear flow field (Fig. 7F), the sense of shear in the R′ fracture zones is opposite to the regional rotation. The opposing sense of rotation from the gross strain field makes R′ shear formation less favorable. This analysis explains why sandbox experiments tend to generate only R shears. It also highlights the importance of the strain state in governing which set of Coulomb fractures may actually develop under finite-strain deformation.

Driving Mechanisms for PGS Deformation

Our understanding of conjugate faults formed under coaxial deformation and R, R′, and P shears formed under noncoaxial deformation was largely derived from analogue experiments. Thus, it is natural to test whether paired general-shear deformation and V-shaped conjugate faults can also be simulated by analogue experiments. A key parameter in setting

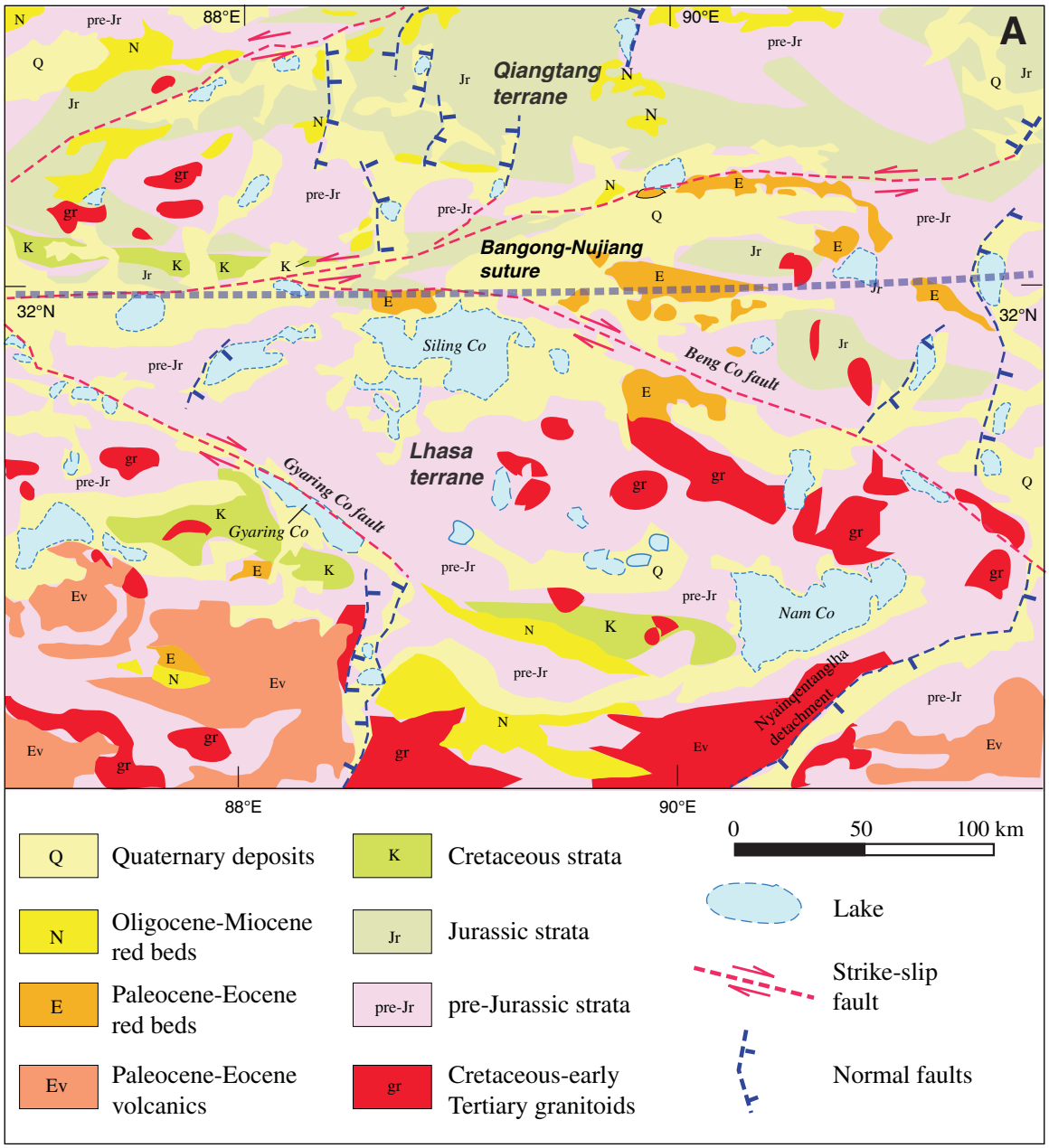

Figure 5 (*Continued on following page*). (A) Simplified geologic map of part of the central Tibet conjugate fault zone compiled from Pan et al. (2004) and Taylor et al. (2003). (B) Geologic map of central Qiangtang terrane showing the relationships between left-slip faults and preexisting structures, simplified from Taylor et al. (2003) and Kapp et al. (2005a).

Geological Society of America Bulletin, published online on 3 March 2011 as doi:10.1130/B30159.1

up the experiments is the appropriate boundary condition. Next, we analyze the Tibetan GPS velocity field using a continuum mechanics approach. This allows us to establish the stress boundary conditions using the Navier-Stokes equations for the current deformation in central Tibet.

Continuum Approximation of the Tibetan GPS Velocity Field

A fundamental mechanism for crystal-plastic deformation is dislocation of crystal lattices. Although this process is not continuous, the bulk deformation of the material under this mechanism is best described by continuum mechanics. This observation may also apply to the active deformation of central Tibet, where individual fault zones at a horizontal dimension of 10 km or less may be treated as discrete structures, while the overall deformation field at a scale of the whole conjugate fault zone (1000–2000 km in width and length) may be best described by continuum mechanics. This approximation implies that whether a region of continental lithosphere deforms in a discrete or continuum fashion depends on the scale we are considering.

Using a local frame of reference (i.e., a fixed Tibet) (Figs. 8A and 8B), we express the velocity component u in the N110°E (x) direction and the velocity component v in the N20°E (y) direction across central Tibet by the following functional forms

$$u = Ax(h^2 - 4y^2) + B, \quad (1a)$$

$$v = -Cy. \quad (1b)$$

The resulting strain-rate field is

$$\dot{\varepsilon}_{xx} = 2Ah, \quad (2a)$$

$$\dot{\varepsilon}_{yy} = -C, \quad (2b)$$

$$\dot{\varepsilon}_{xy} = -4Axy, \quad (2c)$$

and the rotation-rate field is

$$\omega_{xy} = -4Axy. \quad (2d)$$

In these equations, A, B, and C are constants related to the boundary conditions. The y-axis divides the northern left-slip zone from the southern right-slip zone coinciding with the axis of the Tibetan conjugate fault zone (Fig. 8A).

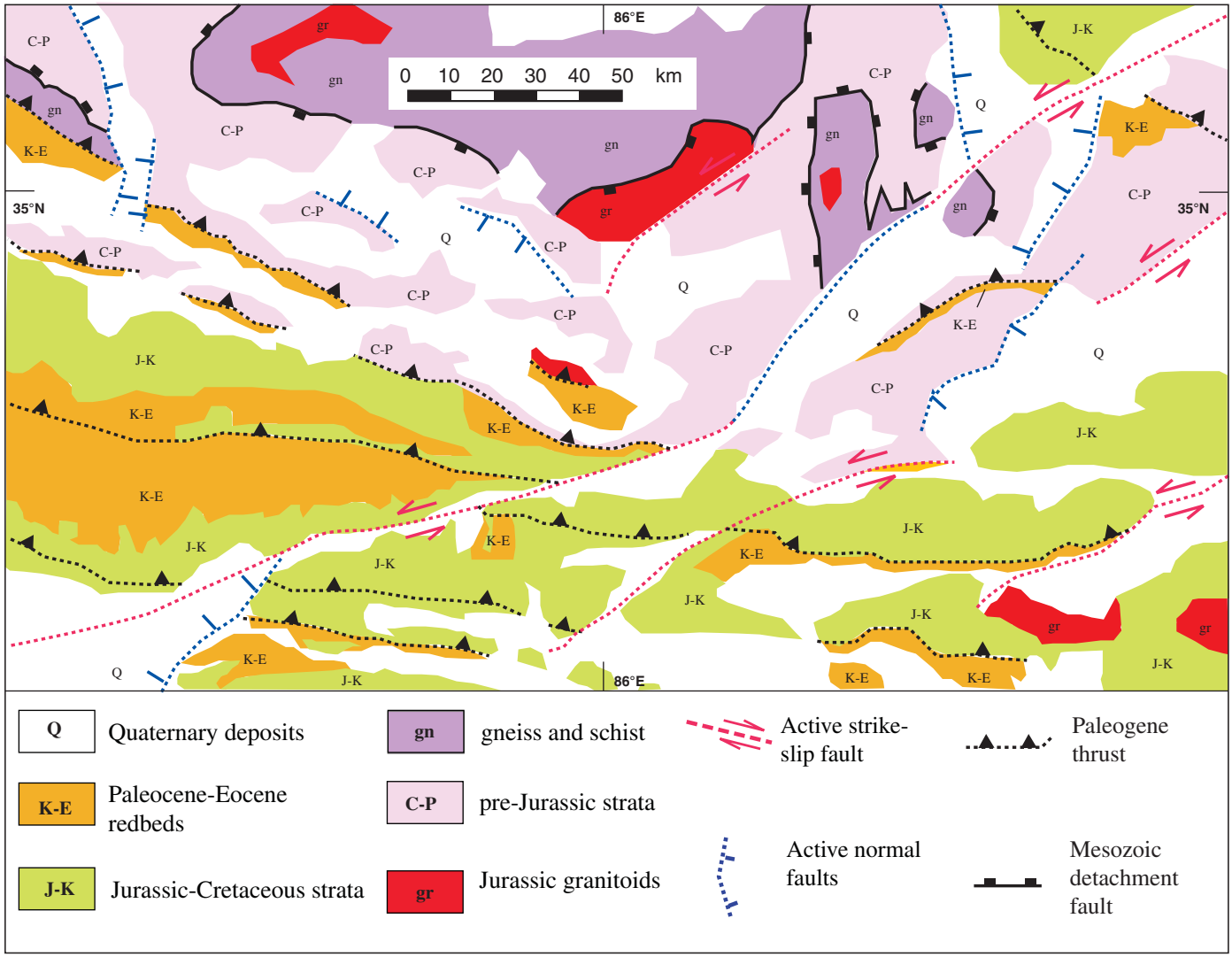

Figure 5 (*Continued*).

Geological Society of America Bulletin, published online on 3 March 2011 as doi:10.1130/B30159.1

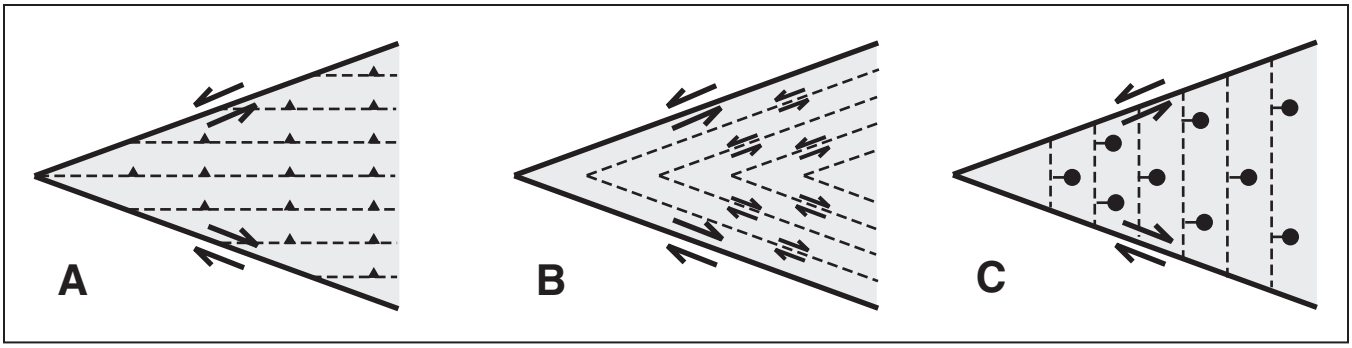

Figure 6. Three possible ways of accommodating vertical-axis rotation via distributed deformation. (A) Distributed thrusting. (B) Distributed conjugate strike-slip faulting. (C) Distributed normal faulting.

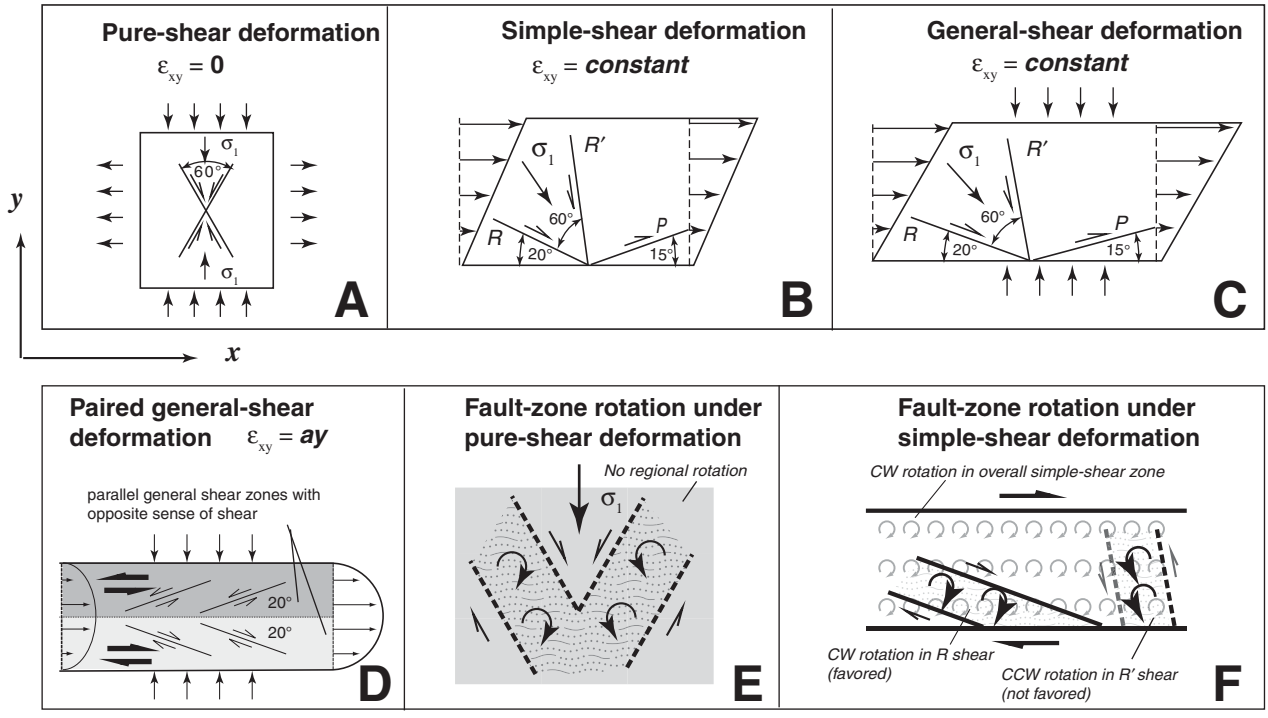

Figure 7. Relationship between state of strain and orientations of fault initiation. (A) Pure-shear deformation and formation of conjugate faults under coaxial deformation. Shear strain on planes perpendicular to the *x* and *y* axes is zero. (B) Simple-shear deformation and formation of Riedel shear (R), conjugate Riedel shear (R′), and primary shear (P). Deformation occurs with the presence of shear strain on planes perpendicular to the *x* and *y* axes. (C) General-shear deformation and formation of Riedel, conjugate Riedel, and primary shears. Deformation occurs with the presence of shear strain on planes perpendicular to the *x* and *y* axes. The shear zone is also under contraction perpendicular to the shear planes. (D) Paired shear zone deformation under which shear strain varies linearly with *y*. (E) Relationship between particle rotation in fault zones and vorticity induced by the regional strain field under coaxial deformation. (F) Relationship between particle rotation in fault zones and vorticity induced by the regional strain field under noncoaxial deformation.

Geological Society of America Bulletin, published online on 3 March 2011 as doi:10.1130/B30159.1

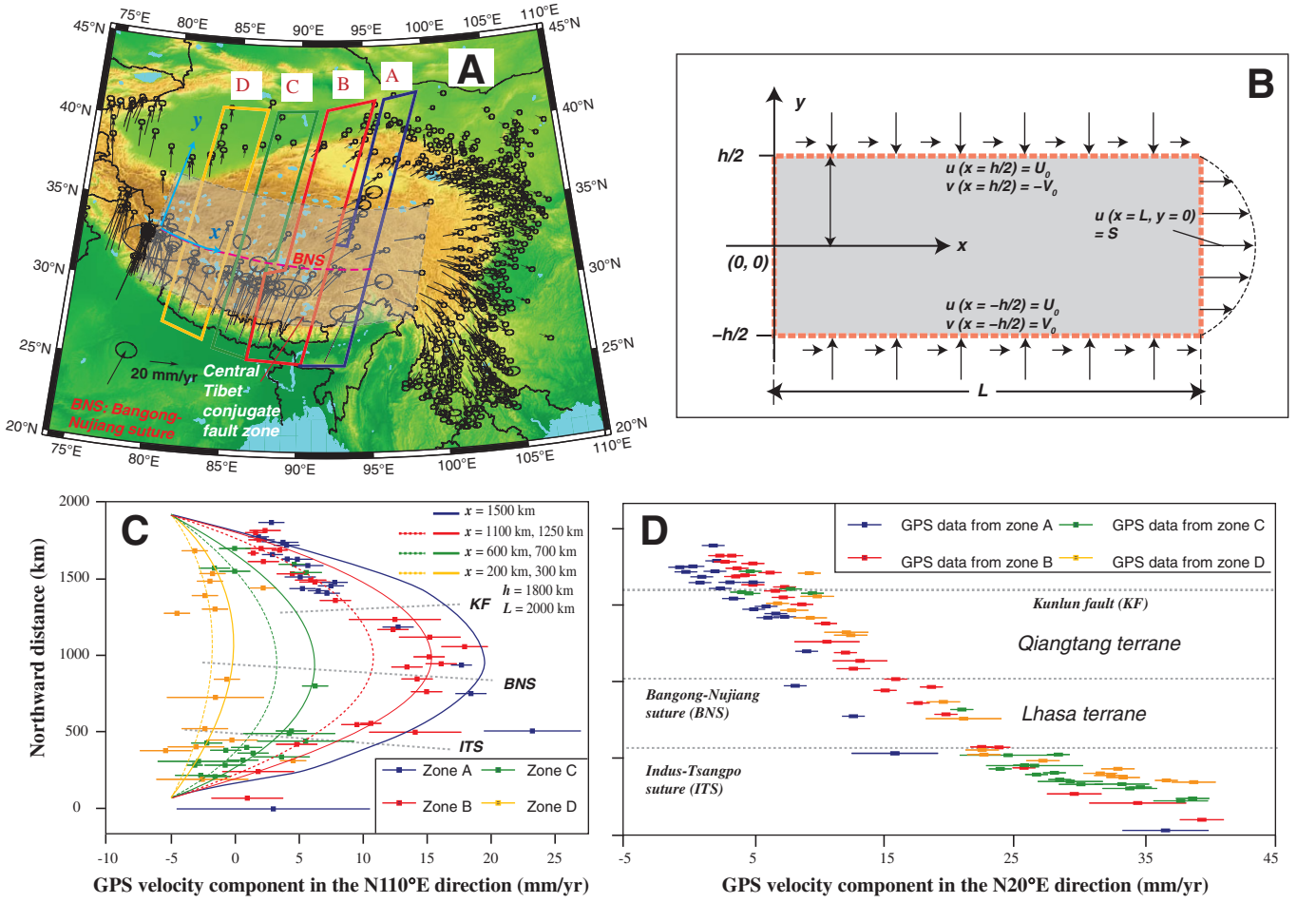

Figure 8. (A) Global positioning system (GPS) velocity field across Tibetan Plateau. Data are mainly from Zhang et al. (2004). Shaded area covers the central Tibet conjugate fault zone. (B) Frame of reference used in this study. Also shown are velocity boundary conditions implied by the GPS data across central Tibet. See text for detailed discussion and derivation. *L*—east-west length of the central Tibet deformation zone; *h*—north-south width of central Tibet deformation zone; *u* and *v*—eastward and northward velocity components; U_0 and V_0—eastward velocity and northward components applied on the northern and southern edge of the deformation zone. (C) Distribution of northward GPS velocity component across Tibet from Zhang et al. (2004). (D) Distribution of eastward GPS velocity component across Tibet from Zhang et al. (2004). (E) Distribution of maximum shear stress and direction of maximum and minimum compressive stress directions derived from GPS velocity field assuming central Tibetan lithosphere is deforming as a Newtonian fluid with a uniform viscosity μ. The magnitude of the maximum shear stress is scaled by μ × 10^{-8} Pa.

Geological Society of America Bulletin, published online on 3 March 2011 as doi:10.1130/B30159.1

Equation 1 requires the following velocity conditions at the northern ($y = h/2$) and southern ($y = -h/2$) margins of Tibet (Fig. 8B); for the northward velocity,

$$v(y = \frac{h}{2}) = -\frac{V_0}{2}, \quad (4a)$$

$$v(y = \frac{h}{2}) = -\frac{V_0}{2}, \quad (4b)$$

and for the eastward velocity component,

$$u(y = \frac{h}{2}) = U_0, \quad (5a)$$

$$u(y = \frac{h}{2}) = U_0, \quad (5b)$$

$$u(x = 0) = U_0. \quad (5b)$$

Equations 4a and 4b represent the velocity boundary conditions for two approaching channel walls, while Equations 5a and 5b represent the eastward velocity on the northern and southern margins of the deforming region in central Tibet (i.e., the shear rates across the northern left-slip and southern right-slip shear zones in the Qiangtang and Lhasa terranes). Finally, Equation 5c represents the velocity at the western edge of the deforming domain in central Tibet. An additional kinematic property implied in Equation 1 is the eastward velocity (i.e., east-west stretching rate) along the x axis at the eastern end of the deformation zone:

$$S = u(y = 0, x = L), \quad (6)$$

where L is the east-west length of the Tibetan deformation zone covered by the GPS surveys (Fig. 8).

Equation 1a has an apparently similar form to that for a Poiseuille flow in an infinitively long channel that has a half-channel width of h in map view. For a Newtonian fluid, this can be expressed as (White, 1986, see p. 323)

$$u = -\frac{1}{8\mu}\frac{dp}{dx}(h^2 - 4y^2), \quad (7)$$

where μ is viscosity, and dp/dx is a constant pressure gradient in the x direction. During Poiseuille flow, the channel walls are fixed, which does not apply to the GPS velocity field across Tibet; there the "channel walls" are moving at a velocity of $\pm V_o$ toward the channel axis. Another difference between Poiseuille flow and the Tibetan GPS velocity field is that the north-south velocity distributions for the latter vary along the x axis from west to east rather than being constant as in the Poiseuille flow. Finally, as shown later in Equation 21a, the pressure gradient that drives the GPS-determined velocity field in central Tibet varies linearly with the x coordinate rather than being constant as in Poiseuille flow. The moving channel boundaries, the flow profiles that vary with the x coordinate, and nonconstant pressure gradient all indicate that the Tibetan GPS velocity field cannot be split into two Couette (i.e., simple-shear) flows with opposite sense of shear.

Using Equations 4, 5, and 6, we can obtain constants A, B, and C in Equations 1 and 2 as

$$A = \frac{S - U_0}{Lh^2}, \quad (8a)$$

$$B = U_0, \quad (8b)$$

$$C = \frac{V_0}{h}. \quad (8c)$$

We now rewrite Equations 1 and 2 as

$$u = \frac{S - U_0}{Lh^2}x(h^2 - 4y^2) + U_0, \quad (9a)$$

$$v = -\frac{V_0}{h}y. \quad (9b)$$

The corresponding strain-rate field is

$$\dot{\varepsilon}_{xx} = \frac{S - U_0}{Lh^2}(h^2 - 4y^2), \quad (10a)$$

$$\dot{\varepsilon}_{yy} = -\frac{V_0}{h}, \quad (10b)$$

$$\dot{\varepsilon}_{xy} = -8\frac{S - U_0}{Lh^2}xy, \quad (10c)$$

where $\dot{\varepsilon}_{xx}$ and $\dot{\varepsilon}_{yy}$ are extension rates in the x and y direction, and $\dot{\varepsilon}_{xy}$ is the shear strain rate. For a Newtonian fluid with a uniform viscosity (μ), the corresponding deviatoric-stress components from the previous equations are:

$$\tau_{xx} = 2\mu\dot{\varepsilon}_{xx} = 2\mu\frac{S - U_0}{Lh^2}(h^2 - 4y^2), \quad (10d)$$

$$\tau_{yy} = 2\mu\dot{\varepsilon}_{yy} = -2\mu\frac{V_0}{h}, \quad (10e)$$

$$\tau_{xy} = 2\mu\dot{\varepsilon}_{xy} = -16\mu\frac{S - U_0}{Lh^2}xy. \quad (10f)$$

Using Equations 10d, 10e, and 10f, we can calculate the maximum horizontal compressive-stress direction by

$$\theta = \frac{1}{2}\arctan[\frac{2\tau_{xy}}{(\tau_{xx} - \tau_{yy})}] = \frac{1}{2}\arctan\{\frac{8(S - U_0)xy}{[(S - U_0)(h^2 - 4y^2) - LhV_0]}\}, \quad (10g)$$

and the maximum shear stress by

$$\tau_{max} = \sqrt{(\frac{\tau_{xx} - \tau_{yy}}{2})^2 + \tau_{xy}^2} = \mu\sqrt{[(\frac{S - U_0}{Lh^2})(h^2 - 4y^2)]^2 + (2\frac{V_0}{h})^2}, \quad (10h)$$

where θ is the angle between the maximum compressive stress and the x axis.

The GPS data of Zhang et al. (2004) imply that the maximum east-west stretching rate along the x axis in Equation 6 is ~24 mm/yr (Fig. 8C); that is, S relative to fixed Eurasia is ~19 mm/yr at $x = L$ and about −5 mm/yr at $x = 0$ (Fig. 8). The left-slip and right-slip shear rate (U_0) relative to fixed Eurasia is about −5 mm/yr (Fig. 8C). The southward and northward velocity toward the east-trending axis of the central Tibet conjugate fault zone (V_0) is ~20 mm/yr. The north-south width of the combined left-slip and right-slip shear zones (h) is ~1800 km, and the east-west length of the paired left-slip and right-slip shear zones (L) is ~2000 km. These parameters enable us to simulate the distribution of eastward velocity across central Tibet along the four swaths of GPS velocity data constructed by Zhang et al. (2004). Note that our modeled curves (Fig. 8C) match best for data from swath B, moderately well for swaths C and D, and not so well for swath A. The main problem with swath D is the lack of GPS data in southern Tibet and across the eastern Himalaya. Also, the presence of active structures bounding the Shillong Plateau in the northeastern Indian continent further complicates the distribution of GPS velocities along swath D. Assuming a plane-strain condition for the current deformation pattern in central Tibet that may be modeled by a Newtonian fluid with a uniform viscosity μ, we obtain the trajectories of maximum and minimum compressive stress directions and the distribution of the maximum shear stress. The results (shown in Fig. 8E) assume L = 2000 km, h = 1800 km, V_0 = 20 mm/yr, U_0 = −5 mm/yr, and S = 19 mm/yr and indicate the presence of two 300-km-wide zones north and south of the symmetry line where the maximum compressive stress is deflected 32°–44° from the north direction. The results also show that the maximum shear stress increases to the northeast and

Geological Society of America Bulletin, published online on 3 March 2011 as doi:10.1130/B30159.1

southeast directions from the origin and reaches maximum values at the northeastern and southeastern corners of the modeled deforming region. The distribution of the maximum compressive stress directions predicts that rifts formed in the Qiangtang and Lhasa terranes should be oriented in the northwest-trending and northeast-trending orientations, respectively, away from the ~300-km-wide, east-trending right-slip and left-slip shear zones (shaded area in Fig. 8E); the deflection angle of the predicted rifts from the north direction for the orientation of pure dip-slip rifts increases from west at N25°E/N25°W to the east at N38°E/N38°W (Fig. 8E). This prediction is generally consistent with NNE-trending rifts in the Lhasa terrane (e.g., Kapp and Guynn, 2004) and explains particularly well the long considered odd NE orientation of the Nyainqentanglha rift in southeast Tibet (Fig. 3). Although some rifts in the Qiangtang terrane are NNW-trending, broadly consistent with the model predictions (Fig. 5B), most rifts in the region are north- or northeast-trending. At least for some of the well-studied Tibetan rifts in the Qiangtang terrane, north-trending rifts tend to occur locally as pull-apart basins linking northeast-striking left-slip faults (Taylor et al., 2003; Fig. 5B). The transition from conjugate strike-slip faulting in the center to rifting to the north and south of central Tibet may have been caused by a switch in the orientation of the intermediate compressive stress; that is, it changes from a vertical orientation in the conjugate strike-slip fault zone to a horizontal orientation outward in the rift zones to the north and south (Fig. 3).

A logical extension of the plain-strain assumption mentioned previously is that the GPS velocity components u and v do not change with depth. This allows us to determine the vertical velocity component w using the continuity equation (i.e., conservation of mass) as shown here:

$$\dot{\varepsilon}_{zz} = \frac{\partial w}{\partial z} = -(\dot{\varepsilon}_{xx} + \dot{\varepsilon}_{yy}) = \frac{V_0}{h} - \frac{S - U_0}{Lh^2}(h^2 - 4y^2), \quad (11)$$

where $\dot{\varepsilon}_{zz}$ is the extension rate in the vertical direction. Integrating Equation 11 yields

$$w = [\frac{V_0}{h} - \frac{S - U_0}{Lh^2}(h^2 - 4y^2)]z + f(x, y), \quad (12)$$

where $f(x, y)$ is an arbitrary function. We determine $f(x, y)$ in Equation 12 using the stress equilibrium equation in the vertical direction as

$$\frac{\partial \sigma_{zz}}{\partial z} + \frac{\partial \sigma_{zx}}{\partial x} + \frac{\partial \sigma_{zy}}{\partial y} - \rho g = 0. \quad (13)$$

Assuming a Newtonian fluid leads to the following relations $\sigma_{zx} = 2\mu\dot{\varepsilon}_{zx}$ and $\sigma_{zx} = 2\mu\dot{\varepsilon}_{zy}$, which can be inserted into Equation 13, where μ is viscosity. Noting that the vertical normal-stress component is lithostatic (i.e., $\sigma_{zz} = \rho g z$), the above operation leads to the following relationship:

$$\frac{\partial^2 f(x, y)}{\partial x^2} + \frac{\partial^2 f(x, y)}{\partial y^2} + 8\frac{S - U_0}{Lh^2} = 0. \quad (14)$$

The general polynomial solution for the equation is

$$f(x, y) = (8\frac{S - U_0}{Lh^2} - b)x^2 + by^2 + cx + dy + exy + f, \quad (15)$$

where b, c, d, e, and f are arbitrary constants. Inserting Equation 15 into Equation 12, we obtain

$$w = [\frac{V_0}{h} - \frac{S - U_0}{Lh^2}(h^2 - 4y^2)]z + (8\frac{S - U_0}{Lh^2} - b)x^2 + by^2 + cx + dy + exy + f \quad (16)$$

Because w is unconstrained from the available GPS data, we cannot determine constants b, c, d, e, and f. However, if the distribution of the vertical velocity across central Tibet has been in a steady state since the initiation of the conjugate fault zone and correlates positively with the topography in central Tibet, then we can make the following simplification for Equation 16. First, the topography in central Tibet is approximately symmetric with respect to the Bangong-Nujiang suture zone in the north-south direction (e.g., Fielding et al., 1994; Taylor et al., 2003) (Fig. 8). That is, $E(x, y, z) = E(x, -y, z)$, where $E(x, y, z)$ and $E(x, -y, z)$ are the elevation distributions of the Tibetan Plateau surface north and south of the Bangong-Nujiang suture zone, respectively. If the topographic symmetry was caused by steady-state uplift, we may assume that the vertical velocity component also has the same symmetry as the topography across the Bangong-Nujiang suture in the form of $w(x, y, z) = w(x, -y, z)$. This symmetry requires constants d and e in Equation 16 to be zero. For the remaining constants, the vertical uplift rate would decrease eastward if c and $(8[U_0 - S]/Lh^2 - b)$ are both negative. Because $U_0 = -5$ mm/yr and $S = 19$ mm/yr (Fig. 7C), $(U_0 - S)/Lh^2$ must be negative. Thus, the value of b in $(8[U_0 - S]/Lh^2 - b)$ under the condition of $(8[U_0 - S]/Lh^2 - b) < 0$ can be either positive or negative, which would imply different boundary conditions as discussed later herein.

Basal Shear

Using Equations 9a, 9b, 16, and 17, we obtain the shear-strain rate components in the z direction as

$$\dot{\varepsilon}_{xz} = \frac{1}{2}(\frac{\partial w}{\partial x} + \frac{\partial u}{\partial z}) = (8\frac{U_0 - S}{Lh^2} - b)x + \frac{c}{2}, \quad (18a)$$

$$\dot{\varepsilon}_{yz} = \frac{1}{2}(\frac{\partial w}{\partial y} + \frac{\partial v}{\partial z}) = by. \quad (18b)$$

These equations indicate that the base of the Tibetan lithosphere (or upper crust, depending on whether and how the crust and mantle are coupled; see further discussion) is experiencing horizontal basal shear that can be decomposed into a top-to-the-west shear and a top-to-the-south shear (or top-to-the-north shear, depending on the sign of constant b) (Fig. 9). Since the basal shear in the north-south direction is most likely induced by northward subduction of Indian continental lithosphere, the sense of

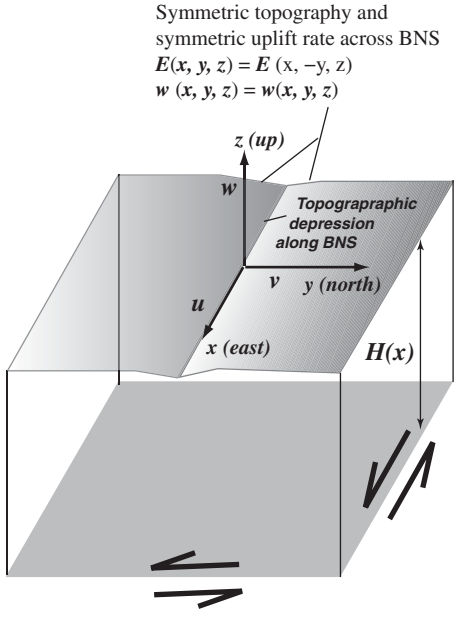

Figure 9. Schematic diagram showing eastward variation of lithospheric thickness (*H*), shear and shear sense at the base of the lithosphere, and east-trending topographic depression along the Bangong-Nujiang suture (BNS) across central Tibet. *E*(*x*, *y*, *z*) represents elevation distribution across the Bangong-Nujiang suture zone, and *w*(*x*, *y*, *z*) represents the inferred distribution of the vertical global positioning system (GPS) velocity component.

Geological Society of America Bulletin, published online on 3 March 2011 as doi:10.1130/B30159.1

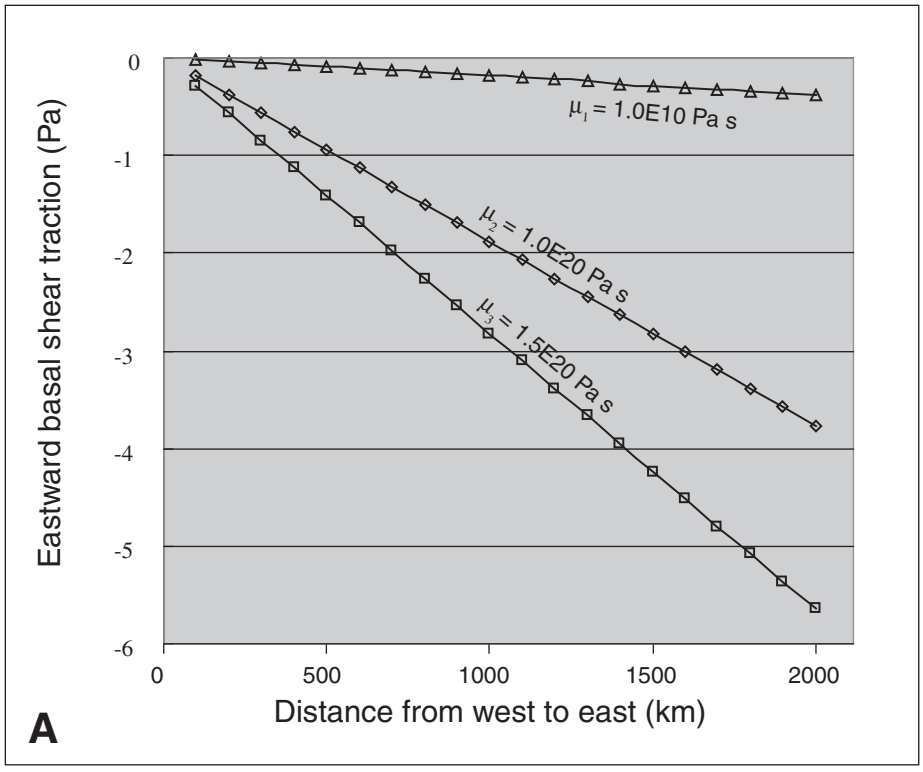

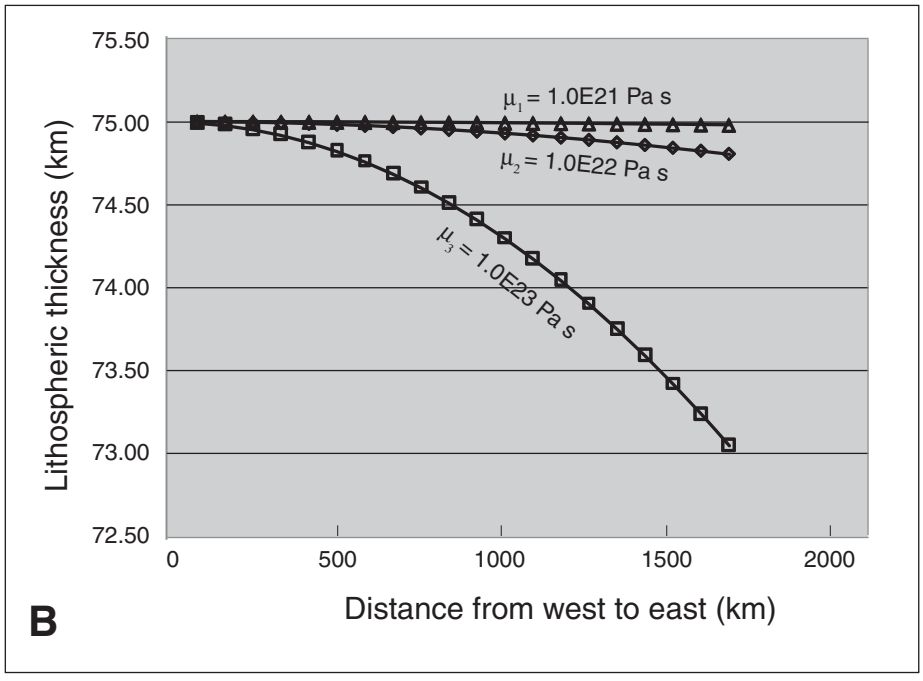

Figure 10. (A) Variation of basal traction in the east-west direction as a function of viscosity. See text for detailed discussion. (B) Variation of Tibetan lithospheric thickness in the east-west direction as a function of average lithospheric viscosity of Tibet. See text for detailed discussion.

shear is most likely top-south, and thus constant b has a negative sign. If central Tibet is only under basal shear in the east direction, then b = 0 in Equation 18, and the eastward basal shear stress becomes

$$\sigma_{xz} = \mu[(16\frac{U_0 - S}{Lh^2})x + c]. \qquad (19)$$

If basal shear stress is zero at the western edge of Tibet, then constant $c = 0$. Equation 19 shows that the absolute value of the basal shear stress increases linearly eastward with x. It is also proportional to viscosity μ and the slip rate U_0 along the northern and southern margins of Tibet. Finally, the basal shear stress is inversely proportional to the length (L) and width (h) of the Tibetan deformation field. This situation was simulated in our sandbox experiments presented later herein. For L = 2000 km, h = 1800 km, $U_0 = -5$ mm/yr, and S = 19 mm/yr, we find that the maximum basal shear traction derived from Equation 19 varies from 5.6 Pa to 3.7 Pa for the average Tibetan viscosity varying from 10^{19} Pa s to 1.5×10^{20} Pa s (Fig. 10A).

Gravitational Spreading

We may also use the analytical functions describing the Tibetan GPS velocity field to explore the role of gravity in driving current Tibetan deformation. Assuming again a simple Newtonian rheology, we can use the following Navier-Stokes equations,

$$-\frac{\partial P}{\partial x} + \mu(\frac{\partial^2 u}{\partial x^2} + \frac{\partial^2 u}{\partial y^2} + \frac{\partial^2 u}{\partial z^2}) = 0 \quad , \quad (20a)$$

$$-\frac{\partial P}{\partial y} + \mu(\frac{\partial^2 v}{\partial x^2} + \frac{\partial^2 v}{\partial y^2} + \frac{\partial^2 v}{\partial z^2}) = 0 \quad , \quad (20b)$$

$$\rho g - \frac{\partial P}{\partial z} + \mu(\frac{\partial^2 w}{\partial x^2} + \frac{\partial^2 w}{\partial y^2} + \frac{\partial^2 w}{\partial z^2}) = 0 \quad , \quad (20c)$$

to derive the following relationships:

$$\frac{\partial P}{\partial x} = -8\mu\frac{S - U_0}{Lh}x \, , \qquad (21a)$$

$$\frac{\partial P}{\partial y} = 0, \qquad (21b)$$

$$\frac{\partial P}{\partial z} = \rho g \, . \qquad (21c)$$

In these equations, g is the gravitational acceleration, and P is the pressure. Because the values

Geological Society of America Bulletin, published online on 3 March 2011 as doi:10.1130/B30159.1

of $\dot{\varepsilon}_{xx}$ and $\dot{\varepsilon}_{yy}$ are both independent of x, σ_{xx} and σ_{yy} should also be independent of x. This leads to the following relationship

$$\frac{\partial P}{\partial x} = -\frac{\partial[(\sigma_{zz} + \sigma_{zz} + \sigma_{zz})/3]}{\partial x} = -\frac{\partial \sigma_{zz}}{3\partial x} = -\frac{\partial(-\rho g z)}{3\partial x}. \quad (22)$$

At the base of the Tibetan lithosphere, Equation 22 combined with Equation 2 can be written as

$$\frac{\partial P}{\partial x} = \frac{\rho g}{3}\frac{\partial H}{\partial x} = -8\mu\frac{S - U_0}{Lh}x. \quad (23a)$$

Rearranging Equation 23a, we obtain

$$\frac{\partial H_L}{\partial x} = -\frac{24\mu(S - U_0)}{\rho g L h^2}x, \quad (23b)$$

where H_L is the thickness of the Tibetan lithosphere. Assuming that the mantle lithosphere thickness is constant in the east-west direction below central Tibet, and only the crustal thickness H_C varies eastward in central Tibet, we can rewrite Equation 23b as

$$\frac{\partial H_C}{\partial x} = -\frac{24\mu(S - U_0)}{\rho g L h^2}x. \quad (23c)$$

Integrating the above equation yields the following relationship:

$$H_C(x) = -\frac{12\mu(S - U_0)}{\rho g L h^2}x^2 + H_0, \quad (24)$$

where H_0 is the crustal thickness at $x = 0$ (i.e., at the western edge of the Tibetan Plateau). Using the parameters obtained from the GPS data (i.e., L = 2000 km, h = 1800 km, S = 19 mm/yr, and U_0 = −5 mm/yr) and assuming the average density of the Tibetan lithosphere of ρ = 2950 kg/m^3 and H_0 = 75 km, we obtain the east-west distribution of Tibetan lithospheric thickness as a function of the average viscosity of the Tibetan lithosphere (Fig. 10B). For a lower viscosity (10^{21} Pa s), the thickness variation is negligible, while for a higher viscosity (10^{23} Pa s), the thickness variation is greater (Fig. 10B). A weaker lithosphere tends to spread laterally and thus keeps its base relatively flat, while a strong lithosphere can support topography and thus maintains a steep gradient of crustal-thickness variation. Even for a viscosity of 10^{23} Pa s for the Tibetan lithosphere, the required crustal-thickness variation is only ~2 km from the eastern to the western end of the Tibetan Plateau (Fig. 10B). Nevertheless, this relationship reveals that such a variation of crustal thickness could drive the formation of a paired general-shear zone in central Tibet. We illustrate this mechanism by using a simple sandbox experiment.

Simulations of PGS Deformation and V-Shaped Conjugate Systems by Analogue Models

Basal Shear Experiments

We used a simple sandbox experiment to demonstrate the role of basal shear in generating V-shaped conjugate faults. In these experiments, we laid a thin layer (~2 cm thick) of fine-grained dry sand over a narrow sliding plate and varied the width of the sliding channel from 1 cm to 5 cm (Fig. 11A). This experiment was capable of generating two sets of Riedel shears with opposing senses of shear in the two adjoining simple-shear zones. It also created a displacement field remarkably similar to the parabolic distribution of the eastward GPS velocity component observed in central Tibet (Fig. 11B). In detail, our sandbox experiments show the following results: (1) No deformation occurs above the sliding plate if the underlying channel is too narrow (i.e., <1.5 cm); (2) Individual Riedel shears form first across the channel margins and then propagate inward. The two sets of Riedel shears eventually merge along the middle line of the channel and form conjugate fault systems. The conjugate faults tend to be linked at their merging points by small normal faults facing the leading edge of the sliding channel; (3) Slip magnitude is greatest on the Riedel shear closest to the leading edge of the sliding plate and decreases systematically to the trailing edge; (4) Each conjugate system develops first near the leading edge of the channel and then propagates backward to the trailing edge; (5) The early formed Riedel shears near the leading edge are rotated the most in an outward sense; this sense of rotation is opposite to the predicted rotation direction for vertical-axis rotation (VAR) models; (6) The distribution of displacement is parabolic in the basal sliding direction, with the maximum magnitude of displacement increasing in the sliding direction.

In several ways, the predictions by our simple sandbox model are consistent with the observations from central Tibet. First, the parabolic distribution of displacement is consistent with the north-south parabolic distribution of the eastward GPS velocity component (Fig. 8C). Specifically, the maximum magnitude of eastward GPS velocity and experimentally determined displacement both increase toward the opening direction of V-shaped conjugate fault systems. Second, the orientations of the simulated Riedel shears are consistent with the observed orientations of the conjugate strike-slip faults in central Tibet. Third, the predicted inward propagation of conjugate faults is consistent with the age distribution of rift initiation across Tibet, which indicates older ages along the margins of the central Tibet deformation zone and younger ages concentrated in the interior of the deformation zone (Fig. 3).

Gravitational Spreading Experiments

Our second experiment was inspired by the vice model of Cruden et al. (2006). We first placed silicon putty with a viscosity of ~5 × 10^{-2} Pa s (e.g., Weijermars, 1986) in a channel (~10 mm deep and 50 mm wide) bounded by two rigid wood boards (Fig. 12A). The silicon putty strip extended only to ~5 mm from the left and ~9 mm from the right end of the channel before the sand layer was placed on top of the channel. This initial condition creates a slight asymmetric boundary condition and affects the final results. The thin sand layer of fine-grained, dry sand had an average thickness of ~8 mm over the silicon putty channel and sloped over the edges of the two rigid wood boards. The width of the overlapping zone between the overlying sand and edges of the wood board was ~5–8 mm.

After the sand layer was added, we fixed the north wall (i.e., the wood board in the upper part of Fig. 12A) and moved the south wall (the wood board in the lower part of the diagram) to the north for a total of 15 mm over about 5 min. This process created two thrust systems with straight traces across the margins of the channel in the overlying sand (Fig. 12B). The sense of thrusting was outward, moving the sand piles over the wood boards. A broad anticline over the viscous channel also developed as the result of contraction, which caused uplift of the silicon putty and raised its top surface above the height of the wood boards. Because the north wall was fixed while the south wall was moving, more silicon putty materials were forced to spread over the south-wall surface. Contraction perpendicular to the channel also caused spreading of the silicon putty laterally parallel to the channel, which moved the lateral ends of the silicon putty strip closer to the two outlets of the channel bounded by the rigid walls.

After moving 15 mm of the south wall relative to the north wall, we fixed the positions of the two wood boards and left the silicon putty in the channel to flow over 24 h under gravity

Geological Society of America Bulletin, published online on 3 March 2011 as doi:10.1130/B30159.1

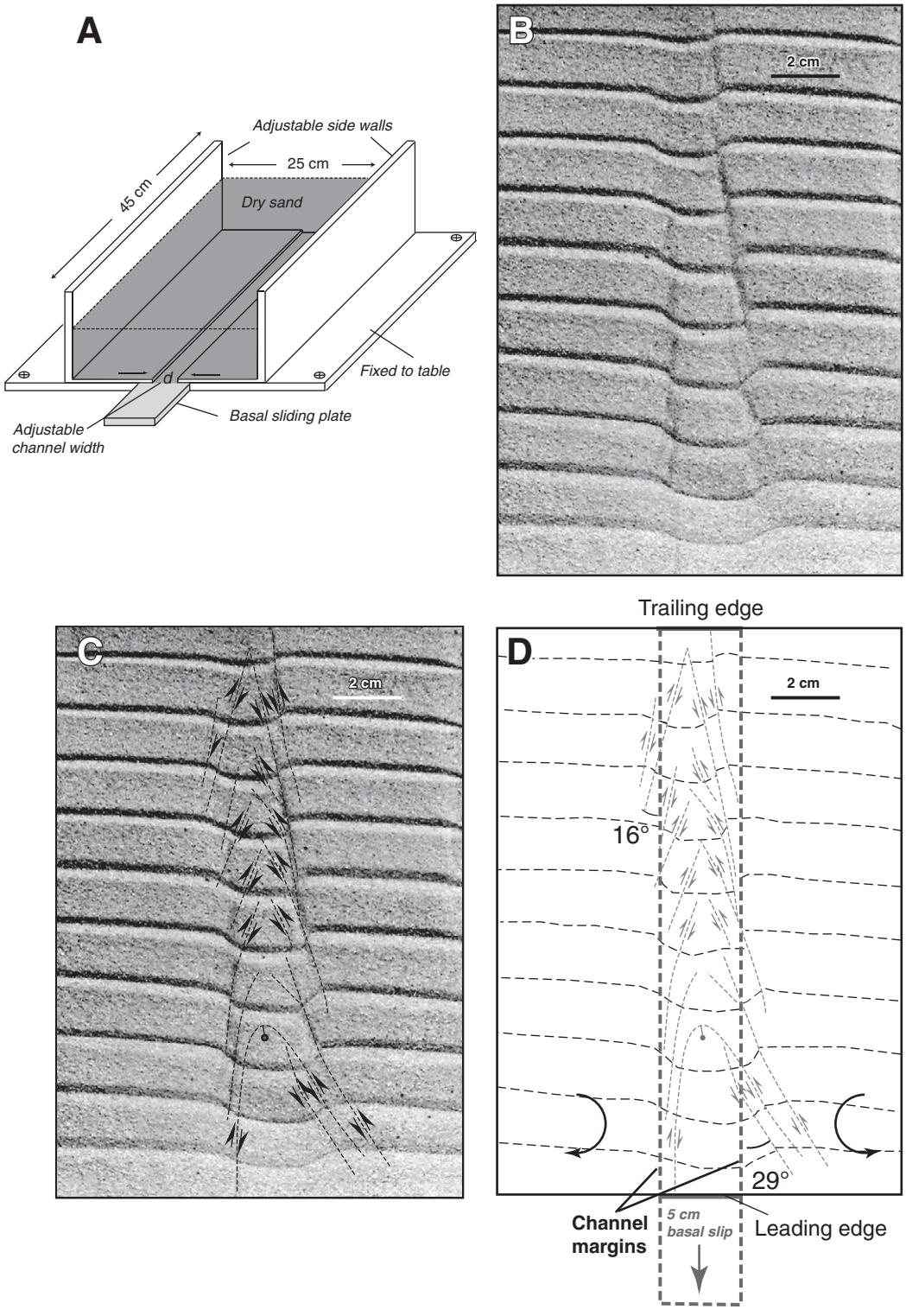

Figure 11. (A) Experimental apparatus to simulate paired shear zones by basal shear. (B) One experiment run under the following condition: 5 cm for the total basal slide and 2 cm for the width of the basal sliding channel. The grooves were originally straight lines deformed into parabolic curves, mimicking the eastward global positioning system (GPS) velocity distribution. The shear-zone width and maximum displacement decrease toward the trailing edge of the channel, and displacement gradient requires channel-parallel extension. Angles between channel margins and simulated Riedel shears generally decrease toward the trailing edge. (C) Interpreted line drawings of the experimental result. (D) Line drawing of the relationship between Riedel shears and underlying sliding channel.

Geological Society of America Bulletin, published online on 3 March 2011 as doi:10.1130/B30159.1

(Fig. 12C). The flow was mainly driven by the change in the thickness of the silicon putty strip at its two ends. The resulting surface displacement field and distribution of faults could be detected by a series of originally straight reference lines on the top of the sand layer (Fig. 12D).

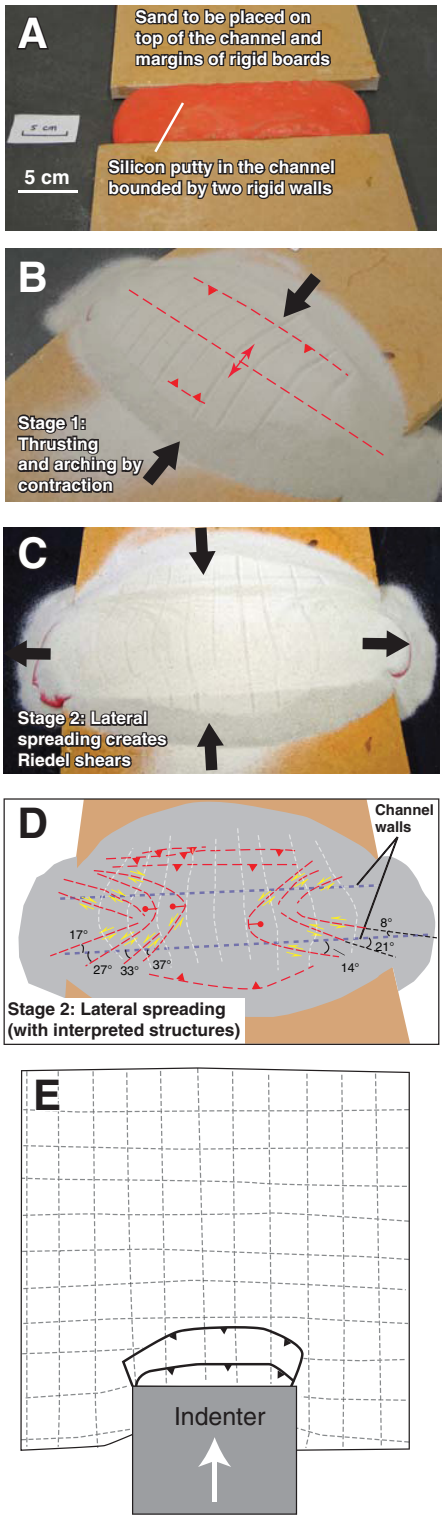

Because of the differences in the initial positions of the lateral ends of the silicon putty strip, the left end of the silicon putty strip traveled farther outside the outlet of the channel than the right end of the silicon putty strip. As a result, the fault patterns on the left and right sides of the deformed sand layer are also slightly different (Fig. 12D). First, although both sides exhibit parabolic distributions of lateral displacements, the maximum displacement is greater on the left side than on the right side of the deforming sand layer. Second, more channel-parallel thrusts are developed on the left side than on the right side.

Although it is less prominent on the right side of the deformed sand layer, the angle between the Riedel shears and the channel margins decreases systematically from the interior outward to the outlets of the channel. On the left side, the angle decreases from 37° to 17°, while on the right side, the angle decreases from 21° to 8° (Fig. 12D). The direction of decrease in the angle between Riedel shears and the channel is opposite to that created by the basal shear experiments (cf. Fig. 11B), in which the angle increases toward the outlet of the channel (i.e., the leading edge of the sliding channel). This difference is created by the different sequence of deformation. For the gravitational spreading experiments, faults formed sequentially from the trailing edge to the leading edge of the basal sliding channel, opposite to those developed in the basal shear experiments. The difference in the sequence of fault development along the flow channel may be used as a criterion to determine which of the two mechanisms operated across central Tibet. The currently available age data from Tibet appears to suggest that the strike-slip faults along the westernmost edge of the central Tibetan deformation zone formed first; that is, they formed at ca. 16 Ma near the western tip of the Kunlun fault and at ca. 20 Ma along the Karakorum fault (Jolivet et al., 2003; Lacassin et al., 2004) (Fig. 3). In the east, the strike-slip faults linking rifts were initiated at about 8 Ma (Harrison et al., 1995). If this age pattern holds up to future scrutiny, it implies that the current deformation field across central Tibet is mainly driven by basal shearing rather than gravitational spreading.

We note that thrusts continued to develop after termination of channel-perpendicular contraction (Fig. 12D; cf. Fig. 12B). This may have resulted from northward and southward spreading of the silicon putty layer over the surfaces of the bounding plates. Of particular interest is the development of an arc-shaped thrust belt in the south over the southern wood board, which had moved relative to the northern wood board during the first stage of deformation in our experiment. This geometry is similar to the observed Himalayan arc, which has not been successfully simulated by analogue experiments (Davy and Cobbold, 1988; Peltzer, 1988). Specifically, the indentation experiments used vertical fronts for the indenter and thus always generated curved thrust belts arching away, rather than toward the indenters as observed in Tibet (Fig. 12E; cf. Fig. 1B). Alternatively, Macedo and Marshak (1999) and Marshak (2004) suggested that arc-shaped thrust belts could be controlled by the three-dimensional shape of the indenter such as an inclined frontal surface.

Problems with Scaling and Comparisons with Early Analogue Experiments

None of the experiments presented here considered scaling (density, viscosity, strain rate, and dimension) (e.g., Hubbert, 1937; Davy and Cobbold, 1991; Cruden et al., 2006). Also, the boundary conditions we used may not correspond exactly to those applied around the Tibetan Plateau in the late Cenozoic. However, we are encouraged by the similarities between the simulated and observed geometry of V-shaped conjugate faults and the GPS-based parabolic velocity field and our simulated parabolic displacement distribution. They suggest that our simple analogue models provide a useful, if not rigorous, guide for deciphering the mechanics of V-shaped conjugate faults.

We also note significant differences between our experimental results and those obtained by Ratschbacher et al. (1991b) in their classic work dealing with a similar problem of simulating distributed extrusion tectonics during indentation of a rigid continental block. Although the analogue experiments of Ratschbacher et al. (1991b) are approximately scaled, there are several important factors appropriate to the Cenozoic development of the Tibetan Plateau that are not considered in their work: (1) time-varying velocity boundary conditions, (2) time-varying viscosity structures in collisional orogens, and (3) the role of basal shear imposed by flow in the lower crust or asthenosphere. Consideration of constant viscosity by Ratschbacher et

Figure 12. Two-layer sandbox experiment for simulating paired general-shear deformation. (A) Silicon putty first filled channel before laying a sand layer on top. (B) Channel-perpendicular compression creates two thrust systems on the channel margins and a broad arch over the channel. (C) Fault pattern and displacement field caused by lateral spreading of the silicon putty. (D) Line drawing of the experimental result. (E) Classic indentation experiments (Davy and Cobbold, 1988) for comparison.

Geological Society of America Bulletin, published online on 3 March 2011 as doi:10.1130/B30159.1

al. (1991a) excludes the possibility of viscosity reduction in the later stages of collisional tectonics and enhanced lateral spreading. A decrease in the average viscosity of the Tibetan lithosphere is expressed by the widespread late Cenozoic volcanism across the plateau, which occurred either coeval with or slightly older than the initiation of the central Tibet conjugate fault zone (e.g., Ding et al., 2003; Chung et al., 2005). The mechanical effect of viscosity reduction can be seen clearly from Equation 21a, in which the pressure gradient driving the observed paired shear-zone flow in central Tibet is proportional to the average viscosity of the Tibetan lithosphere. As its viscosity decreases, the required pressure gradient also decreases, making it easier to drive the eastward flow and thus the formation of the conjugate fault zone. The second factor that distinguishes our experiments from those performed by Ratschbacher et al. (1991b) is the basal boundary conditions. In both experiments performed in our study, this boundary condition is either directly imposed by a sliding plate (Fig. 11) or indirectly imposed by viscous flow of a ductile layer below a dry sand layer (Fig. 12). Such a boundary condition was not considered in the experiments performed by Ratschbacher et al. (1991b). Finally, our two-layer experiment shown in Figure 12 implies that contraction across central Tibet was negligible in the past 14–8 m.y. during the development of the conjugate strike-slip faults in central Tibet, which is possibly related to reduction of convergence rates with time across the Himalayan front. Such a time-varying velocity boundary condition was also not considered in Ratschbacher et al.'s (1991b) experiments. We are currently developing a new experimental apparatus incorporating proper scaling of time-varying viscosity structures, strain rates, dimensions, and time-varying velocity boundary conditions to address these issues more rigorously.

DISCUSSION

Based on geologic observations, we show that late Cenozoic V-shaped conjugate strike-slip faults in central Tibet cannot be explained by a combination of the Coulomb fracturing process and vertical-axis rotation. The observations are also incompatible with formation of the conjugate faults by reactivation of preexisting zones of weakness. Instead, we show that the current deformation field in central Tibet as constrained by GPS data is best described by the presence of two parallel and adjoining general-shear zones that are east-trending and have opposing senses of shear. Because the development of the two shear zones is capable of creating two sets of Riedel shears that match the current orientations of the observed V-shaped conjugate faults, we conclude that the conjugate faults were initiated during the formation of the two parallel shear zones. This interpretation indicates that the GPS-based deformation field has existed in central Tibet since at least 16–8 Ma when the strike-slip faults and linked rifts were first initiated.

Our analysis of the GPS data and the assumption that central Tibet deforms as a homogeneous Newtonian fluid lead to the conclusion that the paired general-shear deformation field was generated by horizontal shear at the base of the Tibetan lithosphere and/or gravitational spreading. We verified the viability of the two mechanisms using simple analogue experiments. Next, we discuss the main implications of our proposed paired general-shear model for fault formation, the corresponding mode of continental deformation, and the relationship between Tibetan crust and the underlying mantle lithosphere.

State of Strain, Fault Formation, and Nature of Continental Deformation

The most important feature of its paired general-shear model is the requirement of noncoaxial deformation in controlling the formation of V-shaped conjugate strike-slip faults (Fig. 7). The main departure of this model from the traditional Anderson fault model (e.g., Anderson, 1942) is that the state of strain is as important as the state of stress in determining the orientations of fault initiation. Specifically, the state of strain controls the selection of Coulomb shear-fracture development in the following manners:

(1) formation of X-shaped classic Coulomb conjugate faults under pure-shear deformation corresponding to the situation of no shear strain (i.e., $d\varepsilon_{xy}/dt = 0$ in the coordinate system shown in Fig. 7A);

(2) formation of conjugate Riedel shears not favored under simple-shear or general-shear deformation corresponding to the situation that shear strain rate is constant ($d\varepsilon_{xy}/dt$ = constant) (Figs. 7B and 7C); and

(3) formation of V-shaped conjugate faults under paired general-shear deformation corresponding to the situation that shear strain rate is a linear function of the spatial coordinate perpendicular to the parabolic flow direction ($d\varepsilon_{xy}/dt = ay$) (Fig. 7D).

In these relationships, $d\varepsilon_{xy}/dt$ is the shear-strain rate applied on planes parallel and perpendicular to the x axis (Fig. 7), and a is an arbitrary constant. Our generalization of the orientations of fault initiation as a function of strain-rate state indicates that formation of X-shaped Coulomb shear fractures is a special case of general-shear deformation. That is, they form when vorticity vanishes (i.e., case 2 in Fig. 7C).

Our proposed correlation between the style of fault initiation and the corresponding state of strain has important dynamic implications for the nonuniqueness of inferred state of stress from the orientation of faults. Specially, if the fault orientation correlates uniquely with a strain state, it does not guarantee the same correlation between the fault orientation and the corresponding stress state, because stress depends on the rheology of the deforming materials when the strain rate is known (see discussion in England and Houseman, 1986). This important implication leads directly to the central issue of the nature of continental deformation: is it fluid-like (continuum deformation) or plate-like (discrete deformation)? Correlation between the state of strain and the formation of V-shaped conjugate faults suggests that where this special class of faults formed, the corresponding mode of lithospheric deformation is best approximated by continuum deformation under general-shear flow. Despite the general consistencies between our results and the England and Houseman model (1986), one should note that the only geologic feature their model was capable of predicting was the final topography of the Tibetan Plateau, aided by assumed convective removal of parts of the mantle lithosphere below Tibet (England and Houseman, 1989). One should also note that the simulated Tibetan Plateau in their model was created based on an assumption that its average elevation was at ~500 m above sea level at the onset of the India-Asia collision, which is inconsistent with the known geologic history of the region (Murphy et al., 1997). Our model, though similar in nature to the England and Houseman model (1986), uses GPS-velocity observations as input, and thus the resulting stress distributions can be compared directly with the observed fault orientations and fault kinematics, a feature that was lacking in the England and Houseman model (1986).

Paired General-Shear Zone Deformation and Generalization of Non-Andersonian Faults

Our proposed paired general-shear zone model may also explain other commonly observed non-Andersonian faults, namely, high-angle reverse faults (e.g., Sibson et al., 1988) and low-angle normal faults (Wernicke, 1992; Lister and Davis, 1989; Yin, 1989) (Fig. 13). The most favorable condition for development of these faults is the presence of a weak zone

Geological Society of America Bulletin, published online on 3 March 2011 as doi:10.1130/B30159.1

capable of ductile flow sandwiched between two relatively rigid blocks moving toward each other (Fig. 13). Using this model, low-angle normal faults may be explained as having initiated in viscous-plastic deformation zones in the middle crust as proposed by Lister and Davis (1989), where rocks are capable of flow and at the same time can develop discrete Riedel shear fractures (Fig. 12A). The required weak crust of the North America Cordillera during the widespread mid-Tertiary development of detachment faults is consistent with the thermal and mechanical state as inferred by Coney and Harms (1984). That is, the thickened Cordillera crust created by the earlier Laramide orogeny was weakened and thus spread laterally due to heating by widespread mantle melting induced by slab rollback of the subducting Farallon plate. Similarly, we suggest that high-angle reverse faults could have formed where a vertical flow channel was present (Fig. 13B). Finally, V-shaped, conjugate strike-slip faults are developed when a paired general-shear zone is developed in map view between two strong regions (Fig. 13C). In central Tibet, the two rigid blocks correspond to the Indian craton in the south and the Kunlun Batholith, Tarim Basin, and Qaidam Basin in the north (Fig. 3).

Depth of Tibetan Conjugate Faults and Flow in the Mantle

In our mechanical analysis, we reach the conclusion that the current velocity field producing paired general-shear deformation could be induced by horizontal basal shear and/or gravitational spreading. In Tibet, we would like to know (1) whether the horizontal shear was applied at the base of the upper crust due to lower-crustal flow or at the base of the mantle lithosphere due to flow in the asthenosphere, and (2) whether gravitational spreading involves only the crust or the whole lithosphere of Tibet. The spatial correlation between the Tibetan GPS velocity field and the V-shaped conjugate faults in central Tibet suggests that the conjugate faults can be used as a proxy for finite-strain deformation under paired general-shear condition. Thus, determining the depth of Tibetan conjugate faults can directly answer these questions.

Simulations of rift-shoulder morphology using an elastic plate model led Masek et al. (1994) to suggest that Tibetan rifting involves only the upper crust. This inference appears to be consistent with shallow seismicity above 10–15 km across most of the Tibetan Plateau (e.g., Molnar and Lyon-Caen, 1989), shallow locking depths of active strike-slip faults (< 20 km; Taylor and Peltzer, 2006), and the presence of bright spots (i.e., local vertical velocity inversion) in the middle crust of Tibet along the INDEPTH seismic reflection lines, which was interpreted to indicate widespread partial melting in the Tibetan middle crust (Nelson et al., 1996; also see review by Klemperer, 2006). This interpretation has led to the suggestion that Tibetan middle crust is weak and highly mobile (Nelson et al., 1996), which in turn stimulated the hypothesis that the Tibetan middle crust is capable of flowing laterally in a channel without inducing significant upper-crustal deformation (Royden, 1996; Royden et al., 1997; Clark and Royden, 2000). As basal shearing is a possible mechanism to induce V-shaped conjugate strike-slip faults in central Tibet, eastward middle-crustal flow with the flow axis along the Bangong-Nujiang suture zone could be the cause for the required basal shear. The correlation between middle-crustal flow and surface deformation would imply strong mechanical coupling between the upper and middle crust in Tibet, which is not consistent with the extreme version of the channel-flow model requiring no shear traction at the base of the brittle upper crust (Clark and Royden, 2000).

Several lines of evidence suggest that the Tibetan crust deforms coherently with the underlying mantle lithosphere in the vertical section. First, lithospheric-scale faulting across Tibet has long been suggested by the offset of the Moho below major strike-slip faults as observed from wide-angle reflection profiles (Hirn et al., 1984). Second, the spatial correlation between active fault traces and fast polarization directions of shear-wave splitting in the upper mantle indicates that the upper crust and the mantle lithosphere are deformed in a coherent fashion (Hirn et al., 1995; Huang et al., 2000; Herquel and Tapponnier, 2005). Third, the involvement of mantle lithosphere (or a strong lower crust, depending on where one places the Moho) in Tibetan deformation is also indicated by the presence of deep earthquakes at depths of 70–90 km in southern Tibet and the Himalaya (e.g., Chen and Kao, 1996; Chen and Yang, 2004; Jackson, 2002; Jackson et al., 2004). Fourth, the wide spacing of major rifts across Tibet also indicates that the rift-bounding faults and their linked conjugate strike-slip faults are lithospheric-scale features (Yin, 2000). Fifth, helium in hot springs from Tibetan rift zones is partially derived from the upper mantle (Hoke et al., 2000), suggesting that the rift-bounding faults cut the whole lithosphere and form a conduit for upward transport of mantle helium. Finally, the compatibility between the finite-strain field inferred from shear-wave anisotropy

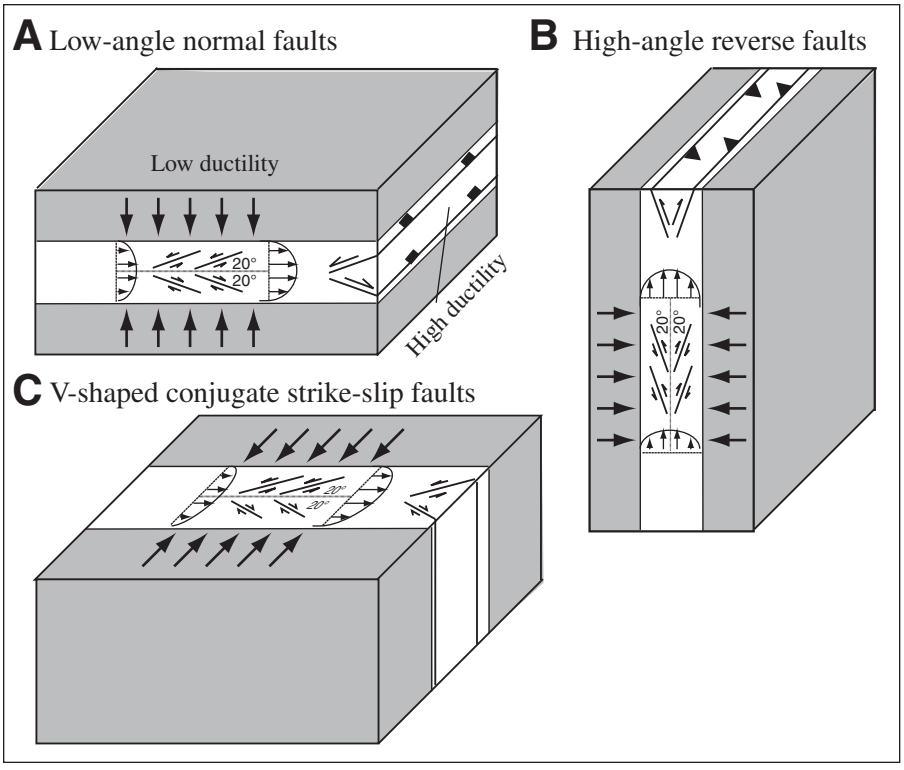

Figure 13. Development of low-angle normal faults (A), high-angle reverse faults (B), and V-shaped conjugate strike-slip faults (C) under paired general-shear deformation.

Geological Society of America Bulletin, published online on 3 March 2011 as doi:10.1130/B30159.1

in the mantle lithosphere and the instantaneous strain-rate field obtained from GPS data further supports vertically coherent deformation in central Tibet (Flesch et al., 2005). The apparent low viscosity of Tibetan middle and lower crust and vertically coherent deformation of the lithosphere can be rationalized in a model developed by Bendick and Flesch (2007), who demonstrated the mechanical plausibility of crust-mantle coupling below Tibet during the India-Asia collision. As pointed out by Yin and Harrison (2000), the INDEPTH profiles imaging bright spots were all surveyed along major active rifts (Nelson et al., 1996), where the presence of hot and potentially weak middle crust is expected due to rift-induced magma injection (Yin, 2000; Kapp et al., 2005b). However, this local observation should not be extrapolated across the entire Tibetan Plateau.

We note that the distribution of the shear-wave splitting time, as summarized in Huang et al. (2000), across Tibet in the north-south direction is approximately parabolic (Fig. 14). That is, the splitting time can be expressed in the following form:

$$t = \frac{t_{\max}}{h_m^{\,2}}(h_m^{\,2} - 4y^2), \qquad (25)$$

where t is the splitting time, t_{max} is the maximum splitting time at $y = 0$, and h_m is the north-south width of the deformation zone in the mantle detected by the shear-wave anisotropy. From the splitting-time data in Figure 13, we find t_{max} is between 1.4 s and 2.2 s, and h_m is ~900 ± 300 km. It appears that the north-south width of the deformation zone in the mantle is only about one half of that for surface deformation derived from the GPS data (i.e., h = 1800 km). If the shear-wave-splitting time measures the magnitude of the east-west stretching strain, Equation 25 indicates that the shear strain varies with y in a parabolic fashion. This functional form is compatible with the distribution of east-west extension strain rate shown in Equation 10a derived from the current GPS velocity field. This reconfirms the conclusion reached by Flesch et al. (2005) that Tibetan lithosphere deforms in a vertically coherent fashion. Because of the large shear-wave-splitting time, it is generally believed that the shear-wave anisotropy originates mostly in the upper mantle (Owens and Zandt, 1997; Davis et al., 1997; Huang et al., 2000; Meissner et al., 2004). However, it remains unclear if the anisotropy was preserved in the Tibetan mantle lithosphere or in the asthenosphere farther below.

We note that the location of the maximum splitting time (i.e., the axis of the parabolic curves approximating the distribution of splitting time) is offset ~150 km north of the Bangong-Nujiang suture zone, where the axis of the central Tibetan conjugate fault zone is located (Fig. 14). There are at least three possible explanations for this offset. First, if the anisotropy was created entirely in the Cenozoic and is located in the mantle lithosphere, the distribution of finite strain recorded in the seismic data could be different from that of instantaneous strain that is recorded in the GPS velocity field and expressed by active conjugate faulting. Second, the anisotropy in the mantle lithosphere could be a combined effect of Cenozoic and pre-Cenozoic deformation. In this case, there should be no correlation between the instantaneous strain field and the finite-strain field in the Tibetan lithosphere. Finally, the Cenozoic anisotropy may be recorded as finite strain in the asthenosphere, with its eastward-flow axis being constantly pushed northward due to low-angle northward subduction of the Indian continental lithosphere. The presence of an east-trending asthenospheric channel below central Tibet sandwiched between the cold Indian and Asian lithosphere has been revealed by numerous

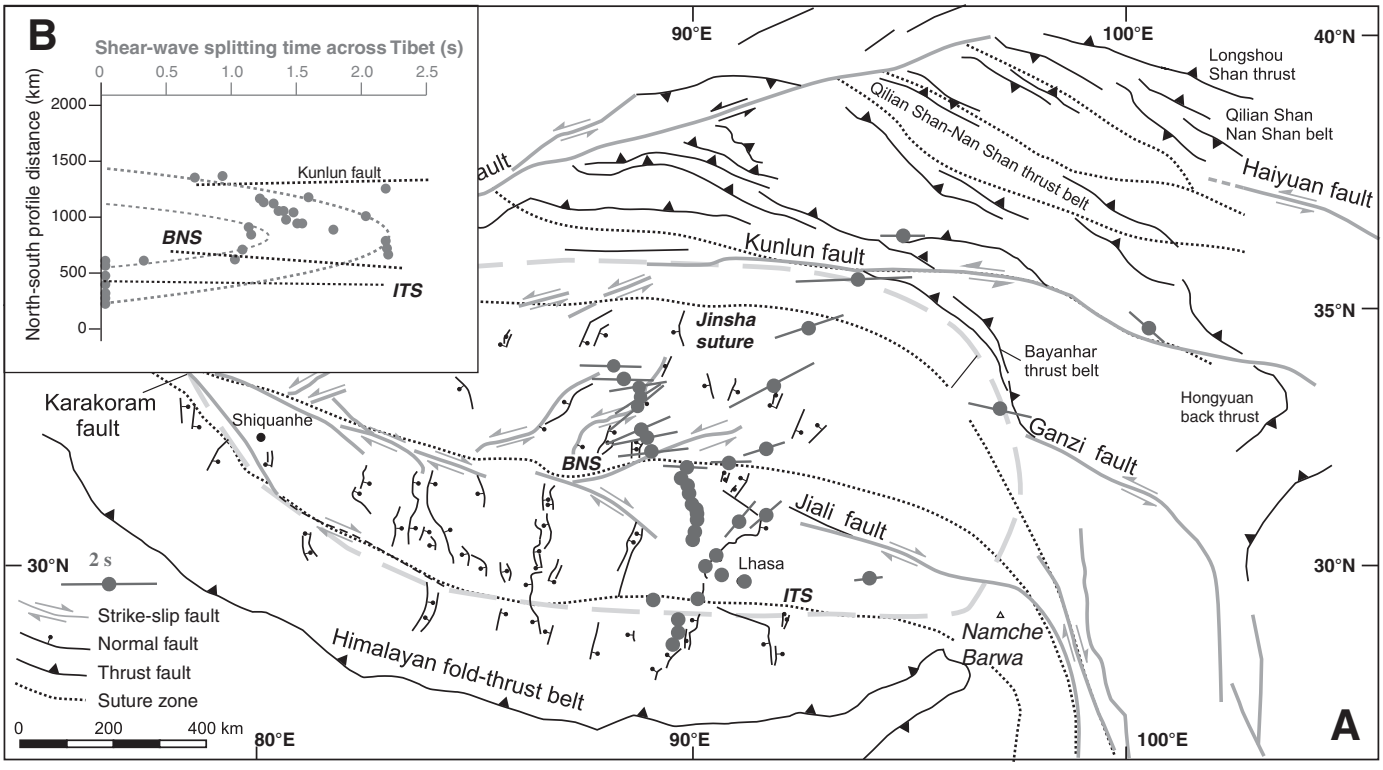

Figure 14. (A) Shear-wave anisotropy across Tibetan plateau (see text for data sources). (B) North-south distribution of shear-wave splitting times across Tibet. Uncertainties are not shown because they are much smaller than their spatial variations. BNS—Bangong Nujiang suture zone; ITS—Indus Tsangpo suture zone.

Geological Society of America Bulletin, published online on 3 March 2011 as doi:10.1130/B30159.1

seismologic studies (e.g., Owens and Zandt, 1997; Kind et al., 2002; Tilmann et al., 2003). Owens and Zandt (1997) and Huang et al. (2000) suggested that it is within this low-velocity zone in the upper mantle that the seismic anisotropy originated. The presence of a low-velocity zone in the upper mantle below central Tibet is also consistent with significantly lower Pn velocities in this region than those in the surrounding areas of the Tibetan Plateau (i.e., India, Tarim, and Sichuan Basin) (Liang et al., 2004). Although we cannot rule out the possibility that options 1 and 2 may contribute to the overall distribution of mantle anisotropy across central Tibet, we consider the third option to be the dominant mechanism in creating mantle anisotropy below central Tibet. This is because of the overwhelming evidence favoring the vertically coherent deformation of lithosphere in central Tibet.

A possible model for the relationship between flow in the mantle and late Cenozoic deformation in the upper crust across central Tibet is shown in Figure 15. In this model, eastward flow of the asthenosphere exerting basal shear together with eastward spreading of the thickened Tibetan lithosphere created paired general-shear deformation in the upper crust of central Tibet. This deformation field caused the development of north-trending rifts in the northern and southern parts of central Tibet and V-shaped conjugate faults in the central part of central Tibet. Underthrusting of the Indian and Asian mantle lithosphere may have caused north-south contraction of the hot and softer asthenospheric channel, which in turn has flowed eastward, inducing basal shear at the base of the Tibetan lithosphere.

Dimension of the PGS Deformation Zone and Distribution of Conjugate Faults

The north-south width of the paired general-shear deformation zone as detected by the GPS data is ~1800 km across the Tibetan Plateau and the Himalayan orogen (Fig. 8A). However, the north-south width of the central Tibetan conjugate fault zone is only ~600–700 km, restricted mostly between the Indus-Tsangpo suture in the south and the Kunlun fault in the north (Fig. 3). This discrepancy raises the question of why the conjugate faults did not extend across most of the Himalayan range in the south and the Qaidam Basin and the Qilian Shan in the north. We attribute this to the spatial variation of mechanical strength mostly controlled by the current thermal state in the lithosphere and a rapid decrease in shear strain rate across the northern and southern parts of the Himalayan orogen. First, the thinner lithosphere below central Tibet as revealed by seismic studies (e.g., Owens and Zandt, 1997; Kind et al., 2002; Tilmann et al., 2003) favors flow-like deformation and thus strike-slip faulting. In contrast, the presence of cold and thick mantle lithosphere below Qaidam Basin and the Himalaya (e.g., Liang et al., 2004) may prevent flow-like deformation and thus the development of Riedel shears. Second, the lack of strike-slip faulting in the northern and southern parts of the Himalayan-Tibetan orogen can be correlated with a decrease in the east-trending shear strain rate in the two regions. This is most obvious in profiles A and B of Zhang et al.'s (2004) GPS data, which cover the most complete sections of the Himalayan-Tibetan orogen. For profile A, shear strain decreases markedly north of the Kunlun fault, which is indicated by a decrease in the northward gradient of the eastward velocity component (Fig. 8C). Similarly, for profile B, the shear strain rate also decreases markedly immediately south of the Indus-Tsangpo suture zone, with nearly undetectable amounts of shear strain when considering the large uncertainties of the GPS measurements (Fig. 8C).

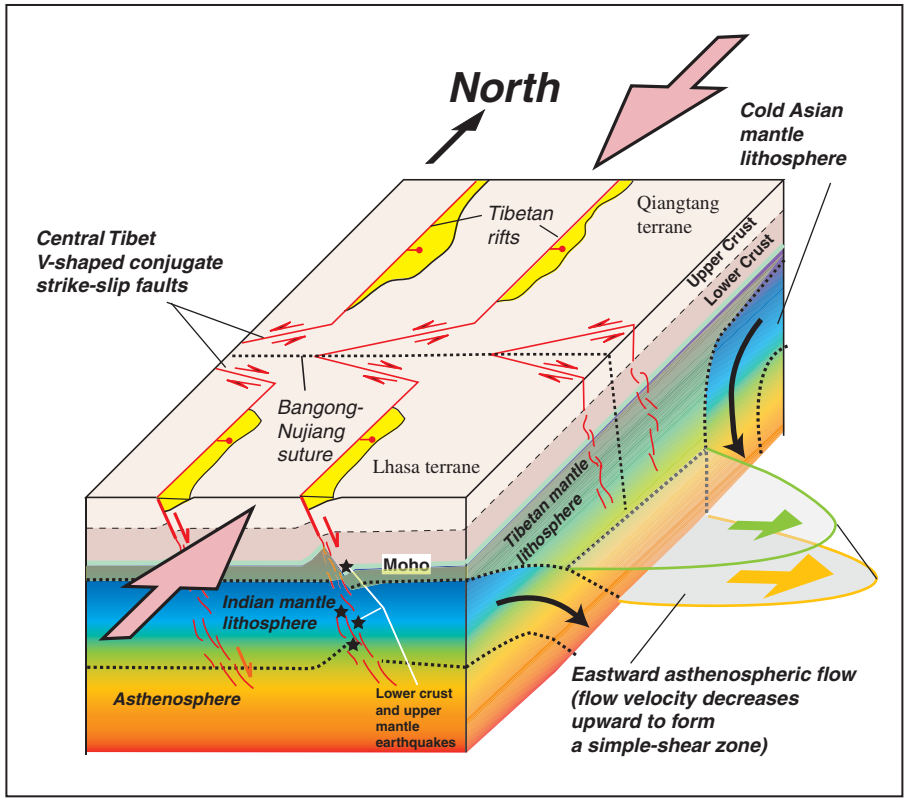

Figure 15. A three-dimensional (3-D) model showing the relationships among V-shaped conjugate strike-slip faults, north-trending rifts, and flow in the lower crust and mantle lithosphere.

Future Tests of the PGS Model

The work presented in this paper represents the first step in understanding the widespread occurrence of V-shaped conjugate strike-slip fault zones in continent-continent collision zones. Further tests are required to confirm or reject the paired general-shear model we propose here. First, we believe that an appropriately scaled analogue model that expands to deal with the formation of non-Anderson dip-slip faults will provide a more complete understanding of strain state versus stress state in controlling the orientations of fault initiation. Second, better GPS coverage is required across central and western Tibet where V-shaped conjugate faults are well developed. As shown in our analysis, the surface distribution of the vertical velocity component has important implications for determining the driving mechanism of the current Tibetan deformation field. Third, precise determination of the vertical distribution of mantle anisotropy below central Tibet will help to resolve whether the shear traction was applied at the base of the upper crust or at the base of the lithosphere. Determination of shear-wave anisotropy along more north-south traverses across all of Tibet will help determine if the strain magnitude varies systematically in

the east-west direction as predicted by the analytical expressions of the paired general-shear model derived from the GPS data. If our model is correct (i.e., Eq. 9a), then east-west extensional strain should be constant from west to east across central Tibet. Finally, paleomagnetic studies on vertical-axis rotation of late Cenozoic Tibetan conjugate faults will provide an ultimate test of our PGS model.

CONCLUSIONS

In this study, we show that the formation of the central Tibet conjugate strike-slip fault zone cannot be explained by vertical-axis rotation or reactivation of preexisting weaknesses. Instead, its formation can be explained by the development of an east-trending left-slip shear zone across the Qiangtang terrane in the north and the development of an east-trending right-slip shear zone in the Lhasa terrane in the south. The formation of the two adjoining shear zones created two sets of Riedel shears: one is oriented in the ENE direction with a left-slip sense of shear and another is oriented in the WNW direction with a right-slip sense of shear. The predicted shear sense and fault orientations match the observed V-shaped conjugate strike-slip faults across central Tibet well. Because the two parallel shear zones also experience synchronous north-south contraction, we term the mechanism for the formation of V-shaped conjugate strike-slip faults the paired general-shear (PGS) model. A detailed analysis of the existing GPS data also suggests that horizontal shear applied at the base of Tibetan mantle lithosphere or lateral spreading of thickened Tibetan lithosphere may have driven late Cenozoic deformation of central Tibet. We verified the mechanical feasibility of the basal-shear and gravitational-spreading mechanisms via simple analogue experiments. Our proposed paired general-shear model implies that the combined effect of the state of strain and the state of stress dictates the style and orientation of fault initiation. Our model also requires that continental lithosphere at a horizontal scale of 1000 km in central Tibet must have deformed in a fluid-like fashion in the late Cenozoic, creating discrete V-shaped conjugate faults over a horizontal scale of a few tens of kilometers.

ACKNOWLEDGMENTS

We thank the donors of the American Chemical Society Petroleum Research Fund for partial support of this research. We also acknowledge support from the Tectonics Program of the U.S. National Science Foundation and the Chinese SINO Probe Project. We thank Richard Styron for helping prepare some of the figures. Constructive comments by Peter Cobbold and Andrew Hynes significantly improved the scientific content and clarity of the paper. Detailed editing by Andrew Hynes and his suggestion of using stress trajectories to illustrate orientations of fault initiation greatly strengthened the science of the paper, for which we are very grateful. A careful read of the final draft by Robby Lovdahl and Sarah Byram has also improved the clarity of the paper.

REFERENCES CITED

Adam, J., Urai, J.L., Wieneke, B., Oncken, O., Pfeiffer, K., Kukowski, N., Lohrmann, J., Hoth, S., van der Zee, W., and Schmatz, J., 2005, Shear localisation and strain distribution during tectonic faulting—New insights from granular-flow experiments and high-resolution optical image correlation techniques: Journal of Structural Geology, v. 27, p. 283–301, doi: 10.1016/j.jsg.2004.08.008.

Alavi, M., 1994, Tectonics of the Zagros orogenic belt of Iran: New data and interpretations: Tectonophysics, v. 229, p. 211–238, doi: 10.1016/0040-1951(94)90030-2.

Allen, M., Jackson, J., and Walker, R., 2004, Late Cenozoic reorganization of the Arabia-Eurasia collision and the comparison of short-term and long-term deformation rates: Tectonics, v. 23, TC2008, doi: 10.1029/2003TC001530.

Allmendinger, R.W., Reilinger, R., and Loveless, J., 2007, Strain and rotation rate from GPS in Tibet, Anatolia, and the Altiplano: Tectonics, v. 26, TC3013, doi: 10.1029/2006TC002030.

Anderson, E.M., 1942, The Dynamics of Faulting and Dyke Formation with Applications to Britain: Edinburgh, Oliver and Boyd, 191 p.

Armijo, R., Tapponnier, P., Mercier, J.L., and Han, T.-L., 1986, Quaternary extension in southern Tibet: Field observations and tectonic implications: Journal of Geophysical Research, v. 91, p. 13,803–13,872, doi: 10.1029/JB091iB14p13803.

Armijo, R., Tapponnier, P., and Han, T., 1989, Late Cenozoic right-lateral strike-slip faulting in southern Tibet: Journal of Geophysical Research, v. 94, p. 2787–2838, doi: 10.1029/JB094iB03p02787.

Backé, G., Dhont, D., and Hervouet, Y., 2006, Spatial and temporal relationships between compression, strike-slip and extension in the central Venezuelan Andes: Clues for Plio-Quaternary tectonic escape: Tectonophysics, v. 425, p. 25–53, doi: 10.1016/j.tecto.2006.06.005.

Bendick, R., and Flesch, L., 2007, Reconciling lithospheric deformation and lower crustal flow beneath central Tibet: Geology, v. 35, p. 895–898, doi: 10.1130/G23714A.1.

Blisniuk, P., Hacker, B., Glodny, J., Ratschbacher, L., McWilliams, M., and Calvert, A., 2001, Normal faulting in central Tibet since at least 13.5 Myr ago: Nature, v. 412, p. 628–632, doi: 10.1038/35088045.

Bourgeois, O., Cobbold, P.R., Rouby, D., and Thomas, J.C., 1997, Least-squares restoration of Tertiary thrust sheets in map view, Tadjik depression, Central Asia: Journal of Geophysical Research, v. 102, p. 27,553–27,573, doi: 10.1029/97JB02477.

Brookfield, M.E., and Hashmat, A., 2001, The geology and petroleum potential of the North Afghan platform and adjacent areas (northern Afghanistan, with parts of southern Turkmenistan, Uzbekistan and Tajikistan): Earth-Science Reviews, v. 55, p. 41–71, doi: 10.1016/S0012-8252(01)00036-8.

Calais, E., Vergnolle, M., San'kov, V., Lukhnev, A., Miroshnitchenko, A., Amarjargal, S., and De'verchère, J., 2003, GPS measurements of crustal deformation in the Baikal-Mongolia area (1994–2002): Implications for current kinematics of Asia: Journal of Geophysical Research, v. 108, doi: 10.1029/2002JB002373.

Casas, A.M., Gapais, D., Nalpas, T., Besnard, K., and Román-Berdriel, T., 2001, Analogue models of transpressive systems: Journal of Structural Geology, v. 23, p. 733–743, doi: 10.1016/S0191-8141(00)00153-X.

Chen, W.P., and Kao, H., 1996, Seismotectonics of Asia: Some recent progress, *in* Yin, A., and Harrison, T.M., eds., The Tectonic Evolution of Asia: Cambridge, UK, Cambridge University Press, p. 37–52.

Chen, W.P., and Yang, Z.H., 2004, Earthquakes beneath the Himalayas and Tibet: Evidence for strong lithospheric mantle: Science, v. 304, p. 1949–1952, doi: 10.1126/science.1097324.

Chung, S.L., Chu, M.F., Zhang, Y.Q., Xie, Y.W., Lo, C.H., Lee, T.Y., Lan, C.Y., Li, X.H., Zhang, Q., and Wang, Y.Z., 2005, Tibetan tectonic evolution inferred from spatial and temporal variations in post-collisional magmatism: Earth-Science Reviews, v. 68, p. 173–196, doi: 10.1016/j.earscirev.2004.05.001.

Clark, M.K., and Royden, L.H., 2000, Topographic ooze: Building the eastern margin of Tibet by lower crustal flow: Geology, v. 28, p. 703–706, doi: 10.1130/0091-7613(2000)28<703:TOBTEM>2.0.CO;2.

Cobbold, P.R., and Davy, P. 1988, Indentation tectonics in nature and experiment. 2. Central Asia: Bulletin of the Geological Institutions of Uppsala, New Series, v. 14, p. 143–162.

Cobbold, P.R., Brun, J.P., Davy, P., Fiquet, G., Basile, C., and Gapais, D., 1989, Some experiments on block rotation in the brittle upper crust, *in* Kissel C., and Laj, C., eds., Paleomagnetic Rotations and Continental Deformation: NATO ASI Series C, Volume 254: Dordrecht, Kluwer Academic Publishers, p. 145–155.

Coleman, M.E., and Hodges, K.V., 1995, Evidence for Tibetan Plateau uplift before 14 Myr ago from a new minimum estimate for east-west extension: Nature, v. 374, p. 49–52, doi: 10.1038/374049a0.

Coney, P.J., and Harms, T.A., 1984, Cordilleran metamorphic core complexes—Cenozoic extensional relics of Mesozoic compression: Geology, v. 12, p. 550–554, doi: 10.1130/0091-7613(1984)12<550:CMCCCE>2.0.CO;2.

Copley, A., and Jackson, J., 2006, Active tectonics of the Turkish-Iranian Plateau: Tectonics, v. 25, TC6006, doi: 10.1029/2005TC001906.

Copley, A., and McKenzie, D., 2007, Models of crustal flow in the India-Asia collision zone: Geophysical Journal International, v. 169, p. 683–698, doi: 10.1111/j.1365-246X.2007.03343.x.

Cruden, A.R., Nasseri, M.H.B., and Pysklywec, R., 2006, Surface topography and internal strain variation in wide hot orogens from three dimensional analogue and two-dimensional numerical vice models, *in* Butler, S.J.H., and Schereurs, G., eds., Analogue and Numerical Modeling of Crustal-Scale Processes: Geological Society of London Special Publication 253, p. 79–104.

Cunningham, D., 2005, Active intracontinental transpressional mountain building in the Mongolian Altai: Defining a new class of orogen: Earth and Planetary Science Letters, v. 240, p. 436–444, doi: 10.1016/j.epsl.2005.09.013.

Davis, G.A., and Burchfiel, B.C., 1973, Garlock fault–Intracontinental transform structure, southern California: Geological Society of America Bulletin, v. 84, p. 1407–1422.

Davis, P., England, P., and Houseman, G., 1997, Comparison of shear wave splitting and finite strain from the India-Asia collision zone: Journal of Geophysical Research, v. 102, p. 27,511–27,522, doi: 10.1029/97JB02378.

Davy, P., and Cobbold, P., 1988, Indentation tectonics in nature and experiment: 1. Experiments scaled for gravity: Bulletin of the Geological Institutions of the University of Uppsala, v. 14, p. 129–141.

Davy, P., and Cobbold, P., 1991, Experiments on shortening of a 4-layer model of the continental lithosphere: Tectonophysics, v. 188, p. 1–25, doi: 10.1016/0040-1951(91)90311-F.

Dewey, J.F., Cande, S., and Pitman, W.C., 1989, Tectonic evolution of the India–Eurasia collision zone: Eclogae Geologicae Helvetiae, v. 82, p. 717–734.

Dhont, D., Chorowicz, J., and Luxey, P., 2006, Anatolian escape tectonics driven by Eocene crustal thickening and Neogene-Quaternary extensional collapse in the eastern Mediterranean region, *in* Dilet, Y., and Pavlides, S., eds., Postcollisional tectonics and magmatism in the Mediterranean region and Asia: Geological Society of America Special Paper 409, p. 331–462.

Ding, L., Kapp, P., Zhong, D.L., and Deng, W.M., 2003, Cenozoic volcanism in Tibet: Evidence for a transition from oceanic to continental subduction: Journal of Petrology, v. 44, p. 1833–1865, doi: 10.1093/petrology/egg061.

Donath, F.A., 1961, Experimental study of shear failure in anisotropic rocks: Geological Society of America Bulletin, v. 72, p. 985–990, doi: 10.1130/0016-7606(1961)72[985:ESOSFI]2.0.CO;2.

Eisenstadt, G., and Sims, D., 2005, Evaluating sand and clay models: Do rheological differences matter: Journal of Structural Geology, v. 27, p. 1399–1412, doi: 10.1016/j.jsg.2005.04.010.

England, P., and Houseman, G., 1986, Finite strain calculations of continental deformation: 2. Comparison with the India-Asia collision zone: Journal of Geophysical Research, v. 91, p. 3664–3676, doi: 10.1029/JB091iB03p03664.

England, P., and Houseman, G., 1989, Extension during continental convergence, with application to the Tibetan Plateau: Journal of Geophysical Research, v. 94, p. 17,561–17,579, doi: 10.1029/JB094iB12p17561.

England, P., and Molnar, P., 1990, Right-lateral shear and rotation as the explanation for strike-slip faulting in eastern Tibet: Nature, v. 344, p. 140–142, doi: 10.1038/344140a0.

Escalona, A., and Mann, P., 2006, An overview of the petroleum system of Maracaibo Basin: The American Association of Petroleum Geologists Bulletin, v. 90, p. 657–678.

Fielding, E., Isacks, B., Barazangi, M., and Duncan, C., 1994, How flat is Tibet: Geology, v. 22, p. 163–167, doi: 10.1130/0091-7613(1994)022<0163:HFIT>2.3.CO;2.

Flesch, L.M., Holt, W.E., Silver, P.G., Stephenson, M., Wang, C.Y., and Chan, W.W., 2005, Constraining the extent of crust-mantle coupling in central Asia using GPS, geologic, and shear wave splitting data: Earth and Planetary Science Letters, v. 238, p. 248–268, doi: 10.1016/j.epsl.2005.06.023.

Fournier, M., Jolivet, L., Davy, P., and Thomas, J.C., 2004, Backarc extension and collision: An experimental approach to the tectonics of Asia: Geophysical Journal International, v. 157, p. 871–889, doi: 10.1111/j.1365-246X.2004.02223.x.

Freund, R., 1970, Rotation of strike-slip faults in Sistan, southeast Iran: The Journal of Geology, v. 78, p. 188–200, doi: 10.1086/627500.

Gan, W.J., Zhang, P.Z., Shen, Z.K., Niu, Z.J., Wang, M., Wan, Y.G., Zhou, D.M., and Cheng, J., 2007, Present-day crustal motion within the Tibetan Plateau inferred from GPS measurements: Journal of Geophysical Research, v. 112, B08416, doi: 10.1029/2005JB004120.

Garzione, C.N., Dettman, D.L., Quade, J., DeCelles, P.G., and Butler, R.F., 2000, High times on the Tibetan Plateau: Paleoelevation of the Thakkhola graben, Nepal: Geology, v. 28, p. 339–342, doi: 10.1130/0091-7613(2000)28<339:HTOTTP>2.0.CO;2.

Guest, B., Pavlis, T.L., Golding, H., and Serpa, L., 2003, Chasing the Garlock: A study of tectonic response to vertical axis rotation: Geology, v. 31, p. 553–556, doi: 10.1130/0091-7613(2003)031<0553:CTGASO>2.0.CO;2.

Guest, B., Axen, G.J., Lam, P.S., and Hassanzadeh, J., 2006, Late Cenozoic shortening in the west-central Alborz Mountains, northern Iran, by combined conjugate strike-slip and thin-skinned deformation: Geosphere, v. 2, p. 35–52, doi: 10.1130/GES00019.1.

Hager, C., Stockli, D., Dewane, T.J., Gehrels, G., and Ding, L., 2007, Timing of magmatism in the Xainza rift, central Lhasa terrane: Evidence for extensional unroofing and exhumation of middle Miocene granites within the central Gangdese batholith: Geological Society of America Abstracts with Programs, v. 39, no. 6, p. 387.

Harrison, T.M., Copeland, P., Kidd, W.S.F., and Lovera, O.M., 1995, Activation of the Nyainquentanglha shear zone: Implications for uplift of the southern Tibetan Plateau: Tectonics, v. 14, p. 658–676, doi: 10.1029/95TC00608.

Herquel, G., and Tapponnier, P., 2005, Seismic anisotropy in western Tibet: Geophysical Research Letters, v. 32, L17306, doi: 10.1029/2005GL023561.

Hirn, A., Hercessian, A., Sapin, M., Jobert, G., Xu, Z.X., Gao, E.Y., Lu, D.Y., and Teng, J.W., 1984, Lhasa block and bordering sutures—A continuation of a 500-km Mono traverse through Tibet: Nature, v. 307, p. 25–27.

Hirn, A., Jiang, M., Sapin, M., Dias, J., Nercerssian, A., Lu, Q.T., LePine, J.C., Shi, D.H., Sachpazi, M., Pandey, M.R., Ma, K., and Gallart, J., 1995, Seismic anisotropy as an indicator of mantle flow beneath the Himalayas and Tibet: Nature, v. 375, p. 571–574, doi: 10.1038/375571a0.

Hoke, L., Lamb, S., Hilton, D.R., and Poreda, R.J., 2000, Southern limit of mantle-derived geothermal helium emissions in Tibet: Implications for lithospheric structure: Earth and Planetary Science Letters, v. 180, p. 297–308, doi: 10.1016/S0012-821X(00)00174-6.

Huang, W.C., Ni, J.F., Tilmann, F., Nelson, D., Guo, J.R., Zhao, W.J., Mechie, J., Kind, R., Saul, J., Rapine, R., and Hearn, T.M., 2000, Seismic polarization anisotropy beneath the central Tibetan Plateau: Journal of Geophysical Research, v. 105, p. 27,979–27,989, doi: 10.1029/2000JB900339.

Hubbert, M.K., 1937, Theory of scale models as applied to the study of geologic structures: Geological Society of America Bulletin, v. 48, p. 3651–3663.

Ivanov, M.A., and Head, J.W., 2008, Formation and evolution of Lakshmi Planum, Venus: Assessment of models using observations from geological mapping: Planetary and Space Science, v. 56, p. 1949–1966, doi: 10.1016/j.pss.2008.09.003.

Jackson, J., 2002, Strength of the continental lithosphere: Time to abandon the jelly sandwich?: GSA Today, v. 12, no. 9, p. 4–10, doi: 10.1130/1052-5173(2002)012<0004:SOTCLT>2.0.CO;2.

Jackson, J., and McKenzie, D., 1984, Active tectonics of the Alpine Himalayan belt between western Turkey and Pakistan: Geophysical Journal of the Royal Astronomical Society, v. 77, p. 185–264.

Jackson, J.A., Austrheim, H., McKenzie, D., and Priestley, K., 2004, Metastability, mechanical strength, and the support of mountain belts: Geology, v. 32, p. 625–628, doi: 10.1130/G20397.1.

Jolivet, L., Davy, P., and Cobbold, P., 1990, Right-lateral shear along the northwest Pacific margin and the India-Eurasia collision: Tectonics, v. 9, p. 1409–1419, doi: 10.1029/TC009i006p01409.

Jolivet, M., Brunel, M., Seward, D., Xu, Z., Yang, J., Malavieille, J., Roger, F., Leloup, A., Arnaud, N., and Wu, C., 2003, Neogene extension and volcanism in the Kunlun fault zone, northern Tibet: New constraints on the age of the Kunlun fault: Tectonics, v. 22, p. 1052, doi: 10.1029/2002TC001428.

Kapp, P., and Guynn, J.H., 2004, Indian punch rifts Tibet: Geology, v. 32, p. 993–996, doi: 10.1130/G20689.1.

Kapp, P., Yin, A., Manning, C.E., Murphy, M., Harrison, T.M., and Spurlin, M., 2000, Blueschist-bearing metamorphic core complexes in the Qiangtang block reveal deep crustal structure of northern Tibet: Geology, v. 28, p. 19–22, doi: 10.1130/0091-7613(2000)28<19:BMCCIT>2.0.CO;2.

Kapp, P., Yin, A., Manning, C., Harrison, T.M., and Taylor, M., 2003a, Tectonic evolution of the early Mesozoic blueschist-bearing Qiangtang metamorphic belt, central Tibet: Tectonics, v. 22, p. 1043, doi: 10.1029/2002TC001383.

Kapp, P., Murphy, M.A., Yin, A., Harrison, T.M., Ding, L., and Guo, J.H., 2003b, Mesozoic and Cenozoic tectonic evolution of the Shiquanhe area of western Tibet: Tectonics, v. 22, no. 4, p. 1029, doi: 10.1029/2001TC001332.

Kapp, P., Yin, A., Harrison, T.M., and Ding, L., 2005a, Cretaceous-Tertiary shortening, basin development, and volcanism in central Tibet: Geological Society of America Bulletin, v. 117, p. 865–878, doi: 10.1130/B25595.1.

Kapp, J.L.D., Harrison, T.M., Kapp, P., Grove, M., Lovera, O.M., and Lin, D., 2005b, Nyainqentanglha Shan: A window into the tectonic, thermal, and geochemical evolution of the Lhasa block, southern Tibet: Journal of Geophysical Research, v. 110, B08413, doi: 10.1029/2004JB003330.

Kind, R., Yuan, X., Saul, J., Nelson, D., Sobolev, S.V., Mechie, J., Zhao, W., Kosarev, G., Ni, J., Achauer, U., and Jiang, M., 2002, Seismic images of crust and upper mantle beneath Tibet: Evidence for Eurasian plate subduction: Science, v. 298, p. 1219–1221, doi: 10.1126/science.1078115.

Klemperer, S., 2006, Crustal flow in Tibet: Geophysical evidence for the physical state of Tibetan lithosphere, and inferred patterns of active flow, *in* Law, R.D., Searle, M.P., and Godin, L. eds., Channel Flow, Ductile Extrusion and Exhumation in Continental Collision Zones: Geological Society of London Special Publication 268, p. 39–70.

Kornsawan, A., and Morley, C.K., 2002, The origin and evolution of complex transfer zones (graben shifts) in conjugate fault systems around the Funan Field, Pattani Basin, Gulf of Thailand: Journal of Structural Geology, v. 24, p. 435–449, doi: 10.1016/S0191-8141(01)00080-3.

Lacassin, R., Valli, F., Arnaud, N., Leloup, P.H., Paquette, J.L., Haibing, L., Tapponnier, P., Chevalier, M.L., Guillot, S., Maheo, G., and Xu, Z.Q., 2004, Large-scale geometry, offset and kinematic evolution of the Karakorum fault, Tibet: Earth and Planetary Science Letters, v. 219, p. 255–269, doi: 10.1016/S0012-821X(04)00006-8.

Leloup, P.H., Lacassin, R., Tapponnier, R., Zhong, D., Lui, X., Zhang, L., and Ji, S., 1995, Kinematics of Tertiary left-lateral shearing at the lithospheric-scale in the Ailao Shan–Red River shear zone (Yunnan, China): Tectonophysics, v. 251, p. 3–10, doi: 10.1016/0040-1951(95)00070-4.

Liang, C.T., Song, X.D., and Huang, J.L., 2004, Tomographic inversion of Pn travel times in China: Journal of Geophysical Research, v. 109, B11304, doi: 10.1029/2003JB002789.

Lister, G.S., and Davis, G.A., 1989, The origin of metamorphic core complexes and detachment faults formed during Tertiary continental extension in the northern Colorado River region, USA: Journal of Structural Geology, v. 11, p. 65–94.

Macedo, J., and Marshak, S., 1999, Controls on the geometry of fold-thrust belt salients: Geological Society of America Bulletin, v. 111, p. 1808–1822, doi: 10.1130/0016-7606(1999)111<1808:COTGOF>2.3.CO;2.

Maheo, G., Leloup, P.H., Valli, F., Lacassin, R., Arnaud, N., Paquette, J.-L., Fernandez, A., Haibing, L., Farley, K.A., and Tapponnier, P., 2007, Post–4 Ma initiation of normal faulting in southern Tibet: Constraints from the Kung Co half graben: Earth and Planetary Science Letters, v. 256, p. 233–243, doi: 10.1016/j.epsl.2007.01.029.

Mandl, G., 1987, Tectonic deformation by rotating parallel faults: The "bookshelf" mechanism: Tectonophysics, v. 141, p. 277–316, doi: 10.1016/0040-1951(87)90205-8.

Mandl, G., 1988, Mechanics of Tectonic Faulting. Models and Basic Concepts: Amsterdam, Elsevier Science Publishers, 407 p.

Mandl, G., and Fernandez Luque, R., 1970, Fully developed plastic shear flow of granular materials: Geotechnique, v. 20, p. 277–307, doi: 10.1680/geot.1970.20.3.277.

Marshak, S., 2004, Salients, recesses, arcs, oroclines, and syntaxes—A review of ideas concerning the formation of map-view curves in fold-thrust belts, *in* McClay, K.R., ed., Thrust Tectonics and Hydrocarbon Systems: American Association of Petroleum Geologists Memoir 82, p. 131–156.

Masek, J.G., Isacks, B.L., Gubbels, T.L., and Fielding, E.J., 1994, Erosion and tectonics at the margins of continental plateaus: Journal of Geophysical Research, v. 99, p. 13,941–13,956, doi: 10.1029/94JB00461.

McGill, S., and Sieh, K., 1991, Surficial offsets on the central and eastern Garlock fault associated with prehistoric earthquakes: Journal of Geophysical Research, v. 96, p. 21,597–21,621, doi: 10.1029/91JB02030.

McGill, S., and Sieh, K., 1993, Holocene slip rate of the central Garlock fault in southeastern Searles Valley, California: Journal of Geophysical Research, v. 98, p. 14,217–14,231, doi: 10.1029/93JB00442.

McKenzie, D., and Jackson, J., 1986, A block model of distributed deformation by faulting: Journal of the Geological Society of London, v. 143, p. 349–353, doi: 10.1144/gsjgs.143.2.0349.

Meissner, R., Tilmann, F., and Haines, S., 2004, About the lithospheric structure of central Tibet, based on seismic: Data from the INDEPTH III profile: Tectonophysics, v. 380, p. 1–25, doi: 10.1016/j.tecto.2003.11.007.

Molnar, P., and Lyon-Caen, H., 1989, Fault plane solutions of earthquakes and active tectonics of the northern and eastern parts of the Tibetan Plateau: Geophysical Journal International, v. 99, p. 123–154, doi: 10.1111/j.1365-246X.1989.tb02020.x.

Montgomery, D.R., Som, S.M., Jackson, M.P.A., Schreiber, B.C., Gillespie, A.R., and Adams, J.B., 2009, Continental-scale salt tectonics on Mars and the origin of Valles Marineris and associated outflow channels: Geological Society of America Bulletin, v. 121, p. 117–133.

Morley, C.K., 2001, Combined escape tectonics and subduction rollback–back arc extension: A model for the evolution of Tertiary rift basins in Thailand, Malaysia and Laos: Journal of the Geological Society of London, v. 158, p. 461–474, doi: 10.1144/jgs.158.3.461.

Morley, C.K., Woganan, N., Sankumarn, N., Hoon, T.B., Alief, A., and Simmon, M., 2001, Late Oligocene–Recent stress evolution in rift basins of northern and central Thailand: Implications for escape tectonics: Tectonophysics, v. 334, p. 115–150, doi: 10.1016/S0040-1951(00)00300-0.

Murphy, M.A., Yin, A., Harrison, T.M., Durr, S.B., Chen, Z., Ryerson, F.J., Kidd, W.S.F., Wang, X., and Zhou, X., 1997, Did the Indo-Asian collision alone create the Tibetan Plateau?: Geology, v. 25, p. 719–722, doi: 10.1130/0091-7613(1997)025<0719:DTIACA>2.3.CO;2.

Naylor, M.A., Mandl, G., and Sijpesteijn, C.H.K., 1986, Fault geometries in basement-induced wrench faulting under different initial stress states: Journal of Structural Geology, v. 8, p. 737–752, doi: 10.1016/0191-8141(86)90022-2.

Nelson, K.D., Zhao, W.J., Brown, L.D., Kuo, J., Che, J.K., Liu, X.W., Klemperer, S.L., Makovsky, Y., Meissner, R., Mechie, J., Kind, R., Wenzel, F., Ni, J., Nabelek, J., Chen, L.S., Tan, H.D., Wei, W.B., Jones, A.G., Booker, J., Unsworth, M., Kidd, W.S.F., Hauck, M., Alsdorf, D., Ross, A., Cogan, M., Wu, C.D., Sandvol, E., Edwards, M., 1996, Partially molten middle crust beneath southern Tibet: Synthesis of Project INDEPTH results: Science, v. 274, p. 1684–1688, doi: 10.1126/science.274.5293.1684.

Owens, T.J., and Zandt, G., 1997, Implications of crustal property variations for models of Tibetan Plateau evolution: Nature, v. 387, p. 37–43, doi: 10.1038/387037a0.

Pan, G.T., Ding, J., Yao, D., and Wang, L., 2004, Geological Map of Qinghai-Xiang (Tibet) Plateau and Adjacent Areas: Chengdu, China, Chengdu Institute of Geology and Mineral Resources, China Geological Survey, Chengdu Cartographic Publishing House, scale 1:1,500,000.

Peltzer, G., 1988, Centrifugal experiments of continental scale tectonics in Asia: Bulletin of the Geological Institutions of the University of Uppsala, v. 14, p. 115–128.

Peltzer, G., and Tapponnier, P., 1988, Formation and evolution of strike-slip faults, rifts, and basins during the India-Asia collision: An experimental approach: Journal of Geophysical Research, v. 93, p. 15,085–15,117.

Powell, R.E., 1993, Balanced palinspastic reconstruction of pre–late Cenozoic paleogeology, southern California: Geologic and kinematic constraints on evolution of the San Andreas fault system, *in* Powell, R.E., Weldon, R.J., II, and Matti, J.C., eds., The San Andreas Fault System: Displacement, Palinspastic Reconstruction and Geological Evolution: Geological Society of America Memoir 178, p. 1–106.

Ratschbacher, L., Merle, O., Davy, P., and Cobbold, P., 1991a, Lateral extrusion in the eastern Alps: 1. Boundary conditions and experiments scaled for gravity: Tectonics, v. 10, p. 245–256, doi: 10.1029/90TC02622.

Ratschbacher, L., Frisch, W., Linzer, H.G., and Merle, O., 1991b, Lateral extrusion in the eastern Alps: 2. Structural analysis: Tectonics, v. 10, p. 257–271, doi: 10.1029/90TC02623.

Richard, P., and Cobbold, P., 1990, Experimental insights into partitioning of fault motions in continental convergent wrench zones: Annales Tectonicae, v. 4, p. 35–44.

Ron, H., Freund, R., Garfunkel, Z., and Nur, A., 1984, Block rotation by strike-slip faulting—Structural and paleomagnetic evidence: Journal of Geophysical Research, v. 89, p. 6256–6270, doi: 10.1029/JB089iB07p06256.

Royden, L., 1996, Coupling and decoupling of crust and mantle in convergent orogens: Implications for strain partitioning in the crust: Journal of Geophysical Research, v. 101, p. 17,679–17,705, doi: 10.1029/96JB00951.

Royden, L.H., Burchfiel, B.C., King, R.W., Wang, E., Chen, Z., Shen, F., and Liu, Y., 1997, Surface deformation and lower crustal flow in eastern Tibet: Science, v. 276, p. 788–790, doi: 10.1126/science.276.5313.788.

Sengor, A.M.C., and Kidd, W.S.F., 1979, Post-collisional tectonics of the Turkish-Iranian Plateau and a comparison with Tibet: Tectonophysics, v. 55, p. 361–376, doi: 10.1016/0040-1951(79)90184-7.

Sibson, R.H., Robert, F., and Poulsen, K.H., 1988, High-angle reverse faults, fluid-pressure cycling, and mesothermal gold-quartz deposits: Geology, v. 16, p. 551–555, doi: 10.1130/0091-7613(1988)016<0551:HARFFP>2.3.CO;2.

Simpson, C., and DePoar, D.G., 1993, Strain and kinematic analysis in general shear zones: Journal of Structural Geology, v. 15, p. 1–20, doi: 10.1016/0191-8141(93)90075-L.

Sylvester, A.G., 1988, Strike-slip faults: Geological Society of America Bulletin, v. 100, p. 1666–1703, doi: 10.1130/0016-7606(1988)100<1666:SSF>2.3.CO;2.

Tapponnier, P., Mattauer, M., Proust, F., and Cassaigneau, C., 1981, Mesozoic ophiolites, sutures, and large-scale tectonic movements in Afghanistan: Earth and Planetary Science Letters, v. 52, p. 355–371, doi: 10.1016/0012-821X(81)90189-8.

Tapponnier, P., Peltzer, G., Le Dain, A.Y., Armijo, R., and Cobbold, P., 1982, Propagating extrusion tectonics in Asia: New insights from simple experiments with plasticine: Geology, v. 10, p. 611–616, doi: 10.1130/0091-7613(1982)10<611:PETIAN>2.0.CO;2.

Tapponnier, P., Peltzer, G., and Armijo, R., 1986, On the mechanics of the collision between India and Asia, *in* Coward, M.P., and Ries, A.C., eds., Collision Tectonics: Geological Society of London Special Publication 19, p. 115–157.

Taylor, M., and Peltzer, G., 2006, Current slip rates on conjugate strike-slip faults in central Tibet using synthetic aperture radar interferometry: Journal of Geophysical Research, v. 111, B12402, doi: 10.1029/2005JB004014.

Taylor, M., and Yin, A., 2009, Active structures of the Himalayan-Tibetan orogen and their relationships to earthquake distribution, contemporary strain field, and Cenozoic volcanism: Geosphere, v. 5, p. 199–214, doi: 10.1130/GES00217.1.

Taylor, M., Yin, A., Ryerson, F., Kapp, P., and Ding, L., 2003, Conjugate strike slip fault accommodate coeval north-south shortening and east-west extension along the Bangong-Nujiang suture zone in central Tibet: Tectonics, v. 22, 21 p., doi: 10.1029/2002TC001361.

Tchalenko, J.S., 1970, Similarities between shear zones of different magnitudes: Geological Society of America Bulletin, v. 81, p. 41–60, doi: 10.1130/0016-7606(1970)81[41:SAOTDB]2.0.CO;2.

Thomas, J.-C., Perroud, H., Cobbold, P.R., Bazhenov, M.L., Burtman, V.S., Chauvin, A., and Sadybakasov, E., 1993, A paleomagnetic study of Tertiary formations from the Kyrgyz Tien-Shan and its tectonic implications: Journal of Geophysical Research, v. 98, p. 9571–9589, doi: 10.1029/92JB02912.

Thomas, J.-C., Chauvin, A., Gapais, D., Bazhenov, M.L., Perroud, H., Cobbold, P.R., and Burtman, V.S., 1994, Paleomagnetic evidence for Cenozoic block rotations in the Tadjik Depression (Central Asia): Journal of Geophysical Research, v. 99, p. 15,141–15,160, doi: 10.1029/94JB00901.

Thomas, J.-C., Cobbold, P.R., Wright, A., and Gapais, D., 1996, Cenozoic tectonics of the Tadzhik Depression, Central Asia, *in* Yin, A., and Harrison, T.M., eds., The Tectonic Evolution of Asia: New York, Cambridge University Press, p. 191–207.

Walker, R.T., Nissen, E., Molor, E., and Bayasgalan, A., 2007, Reinterpretation of the active faulting in central Mongolia: Geology, v. 35, p. 759–762, doi: 10.1130/G23716A.1.

Wernicke, B., 1992, Cenozoic extensional tectonics of the U.S. Cordillera, *in* Burchfiel, B.C., Lipman, P.W., and Zoback, M.L., eds., The Cordilleran Orogen: Conterminous U.S.: The Geology of North America: Boulder, Colorado, Geological Society of America, v. G-3, p. 553–582.

White, F.M., 1986, Fluid Mechanics (second edition): New York, McGraw-Hill Book Company, 732 p.

Wilcox, R.E., Harding, T.P., and Seely, D.R., 1973, Basic wrench tectonics: American Association of Petroleum Geologists Bulletin, v. 57, p. 74–96.

Xizang B.G.M.R. (Xizang Bureau of Geology and Mineral Resources), 1993, Regional Geology of the Xizang Autonomous Region: Beijing, Geological Publishing House, 707 p.

Yin, A., 1989, Origin of regionally, rooted low-angle normal faults—A mechanical model and its tectonic implications: Tectonics, v. 8, p. 469–482, doi: 10.1029/TC008i003p00469.

Yin, A., 2000, Mode of Cenozoic east-west extension in Tibet suggests a common origin of rifts in Asia during Indo-Asian collision: Journal of Geophysical Research, v. 105, p. 21,745–21,759, doi: 10.1029/2000JB900168.

Yin, A., 2010, Cenozoic tectonic evolution of Asia: A preliminary synthesis: Tectonophysics, v. 488, p. 293–325, doi: 10.1016/j.tecto.2009.06.002.

Yin, A., and Harrison, T.M., 2000, Geologic evolution of the Himalayan-Tibetan orogen: Annual Review of Earth and Planetary Sciences, v. 28, p. 211–280, doi: 10.1146/annurev.earth.28.1.211.

Yin, A., Harrison, T.M., Ryerson, F.J., Chen, W., Kidd, W.S.F., and Copeland, P., 1994, Tertiary structural evolution of the Gangdese thrust system, southeastern Tibet: Journal of Geophysical Research, v. 99, p. 18,175–18,201, doi: 10.1029/94JB00504.

Yin, A., Kapp, P.A., Murphy, M.A., Manning, C.E., Harrison, T.M., Grove, M., Ding, L., Deng, X.G., and Wu, C.M., 1999, Significant late Neogene east-west extension in northern Tibet: Geology, v. 27, p. 787–790, doi: 10.1130/0091-7613(1999)027<0787:SLNEWE>2.3.CO;2.

Yin, Z.M., and Ranalli, G., 1992, Critical stress difference, fault orientation and slip direction in anisotropic rocks under non-Andersonian stress systems: Journal of Structural Geology, v. 14, p. 237–244, doi: 10.1016/0191-8141(92)90060-A.

Zhang, P., Shen, Z., Wang, M., Gan, W., Burgmann, R., and Molnar, P., 2004, Continuous deformation of the Tibetan Plateau from global positioning system data: Geology, v. 32, p. 809–812, doi: 10.1130/G20554.1.

Manuscript Received 22 August 2009
Revised Manuscript Received 15 July 2010
Manuscript Accepted 19 July 2010

Printed in the USA